A subtype of olfactory bulb interneurons is required for odor detection and discrimination behaviors

DOI:
10.1523/JNEUROSCI.2783-15.2016

Document Version
Accepted author manuscript

Published in:
Journal of Neuroscience

The Journal of Neuroscience

http://jneurosci.msubmit.net

JN-RM-2783-15R3

A subtype of olfactory bulb interneurons is required for odor detection and discrimination behaviors

Akio Tsuboi, Nara Medical University
Hiroo Takahashi, Nara Medical University
Yoichi Ogawa, Nara Medical University
Sei-ichi Yoshihara, Nara Medical University
Ryo Asahina, Nara Medical University
Masahito Kinoshita, Nara Medical University
Tatsuro Kitano, Nara Medical University
Michiko Kitsuki, Nara Medical University
Kana Tatsumi, Nara Medical University
Mamiko Okuda, Nara Medical University
Kouko Tatsumi, Nara Medical University
Akio Wanaka, Nara Medical University
Hirokazu Hirai, Gunma University
Peter Stern, Paterson Institute for Cancer Research, University of Manchester

Commercial Interest:

The Journal of Neuroscience
Development/Plasticity/Repair
Senior Editor Dr. Mark Bothwell

A subtype of olfactory bulb interneurons is required for odor detection and discrimination behaviors

Abbreviated title: Interneurons for odor detection and discrimination (50 characters)

Hiroo Takahashi[1,6], Yoichi Ogawa[2,6], Sei-ichi Yoshihara[1], Ryo Asahina[1], Masahito Kinoshita[1], Tatsuro Kitano[1], Michiko Kitsuki[1], Kana Tatsumi[1], Mamiko Okuda[1], Kouko Tatsumi[3], Akio Wanaka[3], Hirokazu Hirai[4], Peter L Stern[5], and Akio Tsuboi[1]

[1] Laboratory for Molecular Biology of Neural System, Advanced Medical Research Center, Nara Medical University, Kashihara, Nara 634–8521, Japan
[2] Department of Physiology I, Nara Medical University School of Medicine, Kashihara, Nara 634–8521, Japan
[3] Department of Anatomy II, Nara Medical University School of Medicine, Kashihara, Nara 634–8521, Japan
[4] Department of Neurophysiology, Gunma University Graduate School of Medicine, Gunma 371–8511, Japan
[5] Institute of Cancer Sciences, Paterson Building, University of Manchester, Manchester M20 4BX, United Kingdom
[6] These authors contributed equally to this work

Correspondence should be addressed to Akio Tsuboi, Laboratory for Molecular Biology of Neural System, Advanced Medical Research Center, Nara Medical University, 840 Shijo-cho, Kashihara, Nara 634-8521, Japan, E-mail: atsuboi@naramed-u.ac.jp.

Total: 54 pages, 10 figures

Abstract, 246; Significance Statement, 120; Introduction, 566; Discussion, 1496.

Author contributions: H.T., Y.O., and A.T. designed the research; H.T., Y.O., S.Y., R.A., M.Kin., T.K., M.Kit., Ka.T., and M.O. performed the research; Ko.T., A.W., H.H., and P.L.S. contributed reagents/animals/analytic tools; H.T., Y.O., S.Y., and A.T. analyzed the data; H.T., Y.O., S.Y., and A.T. wrote the paper.

Acknowledgments: This work was supported by Grants-in-Aid for Scientific Research on (B) (A.T.), (C) (H.T. and S.Y.), and Innovative Areas (Adaptive circuit shift) (A.T.), and for Challenging Exploratory Research (A.T.) from the Ministry of Education, Culture, Sports, Science and Technology (MEXT), Japan. A.T. was supported by grants from the Smoking Research Foundation, Japanese Applied Enzymology Foundation, Senshin Medical Research Foundation, and Ono Medical Research Foundation, and a Nara Medical University Grant-in-Aid for Collaborative Research Projects in Japan. H.T. and S.Y. were supported by grants from Takeda Science Foundation and Astellas Foundation for Research on Metabolic Disorders, Japan. H.T. was supported by grants from the Salt Science Research Foundation (no. 14C3), Mishima Kaiun Memorial Foundation, and Banyu Life Science International Foundation in Japan. S.Y. was supported by a grant from Terumo Foundation for Life Sciences and Arts. We gratefully thank Dr. Yasuhiko Saito for electrophysiological analysis, and the animal facility staff of Nara Med. Univ. for their expert assistance.

Correspondence: Correspondence should be addressed to Akio Tsuboi, Laboratory for Molecular Biology of Neural System, Advanced Medical Research Center, Nara Medical University, 840 Shijo-cho, Kashihara, Nara 634–8521, Japan, E-mail: atsuboi@naramed-u.ac.jp.

Abstract

Neural circuits that undergo reorganization by newborn interneurons in the olfactory bulb (OB) are necessary for odor detection and discrimination, olfactory memory, and innate olfactory responses, including predator-avoidance and sexual behaviors. The OB possesses many interneurons, including various types of granule cells (GCs); however, the contribution each type of interneuron makes to olfactory behavioral control remains unknown. Here, we investigated the *in vivo* functional role of oncofetal trophoblast glycoprotein 5T4, a regulator for dendritic arborization of *5T4*-expressing GCs (5T4 GCs), whose level is reduced in the OB of *5T4* knockout mice. Electrophysiological recordings with acute OB slices indicated that external tufted cells (ETCs) can be divided into two types, bursting and non-bursting. Optogenetic stimulation of 5T4 GCs revealed their connection to both bursting and non-bursting ETCs, as well as to MCs. Interestingly, non-bursting ETCs received fewer inhibitory inputs from GCs in *5T4* knockout mice than from those in wild-type mice, while bursting ETCs and MCs received similar inputs in both mice. Furthermore, 5T4 GCs received significantly fewer excitatory inputs in *5T4* knockout mice. Remarkably, in olfactory behavior tests, *5T4* knockout mice had higher odor-detection thresholds than the wild type, as well as defects in odor-discrimination learning. Thus, the loss of 5T4 attenuates inhibitory inputs from 5T4 GCs to non-bursting ETCs and excitatory inputs to 5T4 GCs, contributing to disturbances in olfactory behavior. Our novel findings suggest that among the various types of OB interneuron, the 5T4 GC subtype is required for odor detection and discrimination behaviors.

Significance Statement

Neuronal circuits in the brain include glutamatergic-principal neurons and GABAergic interneurons. Although the latter is a minority cell type, they are vital for normal brain function because they regulate the activity of principal neurons. If interneuron function is impaired, brain function may be damaged, leading to behavior disorder. The olfactory bulb (OB) possesses various types of interneurons including granule cells (GCs); however, the contribution that each type of interneuron makes to the control of olfactory behavior remains unknown. Here, we analyzed electrophysiologically and behaviorally the function of oncofetal trophoblast glycoprotein 5T4, a regulator for dendritic branching in OB GCs. We found that among the various types of OB interneuron, the 5T4 GC subtype is required for odor-detection and odor-discrimination behaviors.

Introduction

Sensory experience plays a crucial role in the development and plastic modification of neural circuits in vertebrates (Lepousez et al., 2013; Nithianantharajah and Hannan, 2006; Sanes and Lichtman, 2001). Specific odorants activate olfactory sensory neurons that express corresponding odorant receptors (Mori and Sakano, 2011). Olfactory sensory neurons project their axons to specific glomeruli in the olfactory bulb (OB) and can subsequently activate a specific neural circuit locally, facilitating dendritic development in interneurons via mitral and tufted cells (MCs/TCs) within the OB (Lepousez et al., 2013; Mori and Sakano, 2011). OB interneurons are generated in the subventricular zone (SVZ) of the lateral ventricle (LV), migrate along the rostral migratory stream, and differentiate into γ-aminobutyric acid (GABA)-releasing inhibitory interneurons, such as granule cells (GCs) and periglomerular cells (PGCs), in the OB throughout life (Adam and Mizrahi, 2010; Kaneko et al., 2010; Lledo et al., 2008; Sakamoto et al., 2011; Whitman and Greer, 2009). Interestingly, adult-born OB interneurons are required for odor detection, odor discrimination, olfactory memory, and innate olfactory responses, including predator-avoidance and sexual behaviors (Alonso et al., 2012; Breton-Provencher et al., 2009; Sakamoto et al., 2011, 2014; Nunes et al., 2015). Odor-evoked activity affects the survival and integration of newborn OB interneurons in pre-existing neural circuits (Lin et al., 2010; Rochefort et al., 2002; Yamaguchi and Mori, 2005). Moreover, olfactory sensory deprivation and odor-rich environments can promote the suppression and acceleration, respectively, of dendritic morphogenesis and spinogenesis of newborn OB interneurons (Livneh et al., 2009; Saghatelyan et al., 2005). Importantly, among various OB interneurons, GCs are the

largest population and are subdivided into several subtypes, based on their morphology and cell lineage (Orona et al., 1983; Merkle et al., 2014; Shepherd et al., 2004); however, the functional specificity that distinguishes each GC subtype remains poorly understood, because of the difficulty in genetically manipulating each OB interneuron subtype alone.

Oncofetal trophoblast glycoprotein 5T4 was first identified in cancer cells (Hole and Stern, 1990). It is expressed at a low level in most normal tissues (Southall et al., 1990), except for the brain and ovary (King et al., 1999; Barrow et al., 2005). We recently identified the *5T4* gene, which is expressed in a unique subtype of OB GCs, termed 5T4 GCs, located in the MC and superficial GC layers (Imamura et al., 2006; Yoshihara et al., 2012). 5T4 regulates the dendritic arborization of 5T4 GCs in a sensory input-dependent manner (Yoshihara et al., 2012). In this study, we performed electrophysiological and behavioral analyses to understand the *in vivo* functional role of 5T4 protein in OB GCs. Electrophysiological recordings with acute OB slices indicated that external tufted cells (ETCs) can be divided into two types, bursting and non-bursting. Photostimulation of *channelrhodopsin2* (*ChR2*)-expressing 5T4 GCs revealed their connection to both bursting and non-bursting ETCs, as well as to MCs. Interestingly, in *5T4* knockout (KO) mice, non-bursting ETCs showed smaller GABAergic inputs evoked by activation of their interacting GCs than in wild-type mice, while bursting ETCs and MCs received similar GABAergic inputs in *5T4* KO and wild-type mice. Notably, *5T4* KO mice, which had less 5T4 GC dendritic branching than wild-type mice, showed remarkably higher odor-detection thresholds and defects in odor-discrimination learning; nevertheless, they were able to detect an odor of interest in the absence of a background odor in both food finding and odor-discrimination

learning tests. These results suggest that 5T4 GC is required for odor-detection and odor-discrimination behaviors.

Materials and Methods

Animals. A *5T4* KO mouse line was generated as described previously (Southgate et al., 2010; RRID:MGI:4459403). The cells were then used to produce chimeric mice and germline progeny; *5T4* heterozygous mice ($5T4^{+/-}$) were backcrossed to the C57BL/6 background. The *5T4* homozygous null ($5T4^{-/-}$) C57BL/6 animals are viable, but adult animals show some structural disorganization within the brain and exhibit a high frequency of hydrocephalus（Southgate et al., 2010). We used $5T4^{-/-}$ male mice for all behavioral tests. Ai32 (*Rosa26—ChR2-enhanced yellow fluorescent protein (EYFP)*) reporter mice, conditionally producing an improved ChR2-EYFP fusion protein, have been described previously (Madisen et al., 2012; RRID:IMSR_JAX:012569).

Generation and injection of lentiviral vectors. Lentiviral vectors were provided kindly by Dr. Nienhuis (St. Jude Children's Research Hospital). Recombinant lentiviral vectors, harboring the *5T4* promoter (6 kb)-driven *gapEYFP* (*5T4p—gapEYFP*) and *5T4p—Cre* constructs, and the *cytomegalovirus* (*CMV*) promoter-driven *gapEYFP* (*CMVp—gapEYFP*) construct, were prepared as described previously (Torashima et al., 2006; Yoshihara et al., 2012). For *5T4* knockdown (KD) experiments, three sets of short hairpin RNAs (shRNAs) targeting the *5T4* gene were prepared as described previously (Yoshihara et al., 2012). As a negative control in the KD experiments, the following three sets of scramble shRNAs were used: scramble sh1, GGTACATATAGCATCTAGATTCAAGAGATCTAGATGCTATATGTACCCTTTT TT; scramble sh2, GATCTGATTCTATGTGTCTTATTCAAGAGATAAGACACA

TAGAATCAGATCTTTTT; and scramble sh3, GCTACTATGCTACTAGTATTATTCAAGAGATAATACTAGTAGCATAGTAGCTTTTT. Neonatal mice at P1–P3 were anesthetized with ice, and then 0.5 µl of lentiviral vector was injected into the LV using an Injection Pump KDS 310 (KD scientific, Holliston, MA, USA). The lentivirus titers were adjusted to 2.0×10^8 TU/ml.

Immunohistochemistry (IHC). Immunohistochemistry (IHC) of mouse OB sections was performed as previously described (Yoshihara et al., 2005, 2012, 2014) using the following antibodies: rabbit anti-GFP antibody (1:1000; Thermo Fisher Scientific Cat# A-11122, RRID:AB_2576216); sheep anti-5T4 antibody (1:1000; R&D Systems Cat# AF5049, RRID:AB_2272148); chicken anti-LacZ (1:1000, Abcam Cat# ab9361, RRID:AB_307210); rabbit anti-cholecystokinin (CCK8) antibody (1:1000; Sigma-Aldrich Cat# C2581, RRID:AB_258806); mouse anti-PGP9.5 antibody (1:100; Abcam Cat# ab8189, RRID:AB_306343); rat anti-BrdU antibody (1:1000; Abcam Cat# ab6326, RRID:AB_305426). DyLight 488- , DyLight 549-, and DyLight 649-conjugated secondary antibodies were purchased from Jackson ImmunoResearch (West Grove, PA, USA). DAPI nuclear counterstaining was performed on all OB sections. Images were acquired using an IX71 microscope (Olympus) equipped with a CCD camera DP30BW (Olympus) or a confocal laser microscope (FV1000-D; Olympus). Stacked images in the X-Y plane from individual thin-sectioned slices were superimposed using Adobe Photoshop to reveal the entire morphology of the cells.

In situ *hybridization (ISH).* Single and double *in situ* hybridization (ISH) were

performed as previously described (Tsuboi et al., 1999; Serizawa et al., 2006; Yoshihara et al., 2012). The coding regions of *5T4* (434–1714 nt; GenBank no. NM_001164792.1) and *cFos* (301–1500 nt; GenBank no. NM_010234.2) were used as templates for digoxigenin- or fluorescein-labeled RNA probes (Roche Diagnostics).

BrdU labeling and detection. To determine the number of newly generated cells, a marker of cell proliferation, 5-bromo-2-deoxyuridine (BrdU; at 10 mg/ml; Nacalai Tesque) was administered intraperitoneally (100 μg/g of body weight dissolved in phosphate-buffered saline (PBS)). After 14 days, the BrdU-labeled cells were detected as described previously (Ishii et al., 2004).

Golgi-Cox staining. The Golgi-Cox method was used to stain neurons as previously described (Ranjan et al., 2010). The following criteria were used for identification of each cell type. ETCs were identified based on their location between the glomerular layer and external plexiform layer (EPL), their larger cell body compared with that of interneurons (>20 μm), and the elongation of their axons to the deeper EPL (Shepherd et al., 2004). MCs were identified based on their location in the MCL, their larger cell body compared with that of the GCs (>20 μm), and the elongation of their axons to the internal plexiform layer.

Acute slice preparation. Mice at 4–6 weeks old (P28–P42) were anesthetized with isoflurane and decapitated. The brain was removed and rapidly immersed in ice-cold solution (composition in mM: sucrose 230, KCl 2.5, $NaHCO_3$ 25, NaH_2PO_4 1.25, $CaCl_2$ 0.5, $MgSO_4$ 10, D-glucose 10) bubbled with 95% O_2/5% CO_2. Slices were cut in this

solution with a vibrating tissue slicer (Vibratome 1000 Plus 102, Pelco International, Redding, CA, USA) and incubated in a standard artificial cerebrospinal fluid (normal ACSF, composition in mM: NaCl 125, KCl 2.5, $NaHCO_3$ 25, NaH_2PO_4 1.25, $CaCl_2$ 2.0, $MgCl_2$ 1.0, D-glucose 25) bubbled with the same mixed gas at 32°C for at least 1 hr.

Whole-cell recordings. Slices were perfused with gas-saturated ACSF at 2–3 ml/min at 32°C. Both the location and shape of each cell were visualized using an upright microscope (BX50WI, Olympus, Tokyo, Japan) equipped with an infrared CCD camera (C2741-79, Hamamatsu Photonics, Hamamatsu, Japan). We defined TCs, whose cell bodies are located within the glomerular layer or in the glomerular layer near the EPL border, as ETCs (Macrides and Schneider, 1982; Shepherd et al., 2004), and analyzed their electrophysiological properties. ETCs were voltage-clamped in the conventional whole-cell configuration using a patch-clamp amplifier (EPC 9, Heka, Lambrecht, Germany). Patch pipettes were pulled from borosilicate glass using a two stage vertical puller (PP-830, Narishige, Tokyo, Japan). To record $GABA_A$ receptor-mediated postsynaptic currents ($GABA_A$-PSCs), the pipettes were filled with high chloride intracellular solution (composition in mM: K-gluconate 95, KCl 50, $MgCl_2$ 2, disodium phosphocreatine 10, Mg-ATP 2, Na_2-GTP 0.3, $CaCl_2$ 0.16, EGTA 3.0, HEPES 10, pH 7.25 with KOH). The calculated Cl^- equilibrium potential is -23.8 mV at 32°C. All membrane potentials were corrected for a 7 mV liquid junction potential measured according to the method of Neher (1992). To block AMPA/KA receptor-mediated currents, CNQX (10 μM) was added to ACSF.

To record excitatory postsynaptic currents (EPSCs), the pipettes were filled with intracellular solution (composition in mM: K-gluconate 121, KCl 4, $MgCl_2$ 2, disodium

phosphocreatine 10, Mg-ATP 2, Na_2-GTP 0.3, $CaCl_2$ 0.16, EGTA 3.0, HEPES 10, pH 7.25 with KOH). Membrane potentials were corrected for a 13 mV liquid junction potential. To block $GABA_A$ receptor-mediated currents, picrotoxin (50 μM) was added to ACSF.

Light stimulation. A lentiviral vector carrying the *5T4p—Cre* construct was injected into both LVs and OBs from Ai32 heterozygous mice (Madisen et al., 2012) at P1. After 4–7 weeks (P28–P49), acute slices were prepared and subjected to recording light-evoked $GABA_A$-PSCs. For photostimulation, a 455 nm LED lamp (M455F1, ThorLabs, NJ, USA) controlled by a LED driver (DC2100, ThorLabs) was used to irradiate with light a circular region with a radius of 100 μm through a 40× objective lens (LUMPlanFI/IR, Olympus). The intensity of the light was measured by an optical power meter (3664, Hioki E. E., Japan) equipped with an adapter (IX3-EXMAD, Olympus). To activate 5T4 GCs expressing *ChR2-EYFP*, either a portion between the surface and intermediate EPLs for recording an ETC, or a portion between the underneath of the MC layer and the surface of the GC layer for recording an MC, was irradiated by light (10–15 ms in duration) at a dose of 10.6 mW/mm^2 in the presence of an 800 mA driving current.

Electrical stimulation. Electrically evoked $GABA_A$-PSCs were recorded under the same conditions as for light-evoked $GABA_A$-PSCs. $GABA_A$-PSCs were evoked by applying constant current stimuli (200 μs in duration) using a bipolar platinum electrode (50 μm in diameter, coated with urethane), which was arranged between the surface and intermediate EPLs for recording an ETC, or between the underneath of the MC layer

and the surface of GC layer for recording an MC. Stimulus intensity was increased in steps of 2 μA from the threshold up to 20 μA, whose stimulation intensity did not directly activate the recorded ETC or MC. At each stimulus intensity, more than 20 stimuli were delivered at an interval of 5 s. The threshold was defined as the stimulus current at which PSCs having an amplitude of more than 25 pA were elicited at a success rate of 25% or more. To study the effect of a single GC on its interacting ETCs or MCs, recordings containing PSC waveforms with a multi-tiered fall were discarded from the analysis, because these waveforms appeared to be a summation of two or more PSCs derived from different GCs. Since the amplitudes of electrically evoked $GABA_A$-PSCs varied considerably from cell to cell, Mann-Whitney rank-sum test was performed to examine for statistical significance.

Electrically evoked EPSCs were recorded at a holding potential of -80 mV. In $5T4^{-/-}$ OB slices, GCs were recorded using a pipette solution containing 100 μM fluorescein digalactoside (FDG). LacZ-positive GCs, namely 5T4-derived GCs, were identified by fluorescence thorough the hydrolysis of FDG after establishing whole-cell configuration. In wild-type OB slices, 5T4 GCs were identified by whole-mount immunostaining with 5T4 antibody after recording the cells. To record a 5T4 GC, the bipolar platinum electrode was arranged between the deep GL and the superficial EPL to stimulate ETCs. The stimulation procedure was similar to that for electrically evoked $GABA_A$-PSCs except for the threshold criteria. Since distinct and stable EPSCs with an amplitude of less than 25 pA were frequently observed in many GCs, the threshold was defined as the stimulus current at which EPSCs having an amplitude of more than 10 pA were elicited at a success rate of 25% or more.

Cell labeling. The internal solution usually contained 1.5% biocytin for morphological examinations. After pipette withdrawal, slices were fixed in 4% paraformaldehyde in 0.1 M PBS overnight. After overnight permeabilization with 0.25% Triton X-100 in PBS, slices were incubated with streptavidin-conjugated Alexa 488 (diluted 1:300 with PBS containing 0.1% Triton X-100) for 6 hr. The slices were then rinsed and mounted in Vectashield (Vector Laboratories, Burlingame, CA, USA). The biocytin-labeled cells were imaged with a confocal laser scanning microscope (FV1000, Olympus, Tokyo, Japan).

Whole-mount immunostaining. Fixed slices were pretreated, as described previously (Renier et al., 2014) with some modifications. Briefly, slices were washed in PBS for 30 min twice, then in 50% methanol (in PBS) for 10 min, 80% methanol for 10 min, and 100% methanol for 30 min twice. After overnight bleaching with 5% H_2O_2, 20% DMSO (in methanol) at 4°C, slices were washed in 100% methanol for 10 min, then in 20% DMSO (in methanol) for 30 min, 80% methanol (in PBS) for 10 min, 50% methanol for 10 min, and PBS for 30 min. Slices were incubated in 20% DMSO, 0.3 M glycine in PBS containing 0.2% Triton X-100 (PBST) at 37°C overnight, and blocked with 10% horse serum in PBST for 2 hr. Pretreated slices were incubated with sheep anti-5T4 antibody (1:1000; R&D Systems), diluted with 1% horse serum, 0.01% sodium azide in PBST, for 16 hr at room temperature. After washing with PBST for 8 hr, slices were incubated with the secondary antibodies (Jackson ImmunoResearch) for 16 hr at room temperature. After washing with PBST for 8 hr, slices were mounted and observed under a confocal laser scanning microscope (FV1000, Olympus).

315 ***Food finding behavior test.*** A food finding behavior test was performed to assess the
316 general ability for olfactory detection, as described previously (Le Pichon et al., 2009)
317 with some modifications. Briefly, before testing, mice were fasted in their home cage
318 for 12 hr, and three successive trials (1st–3rd) were conducted at 1 hr intervals. In the
319 1st and 2nd trials, a food pellet was buried at the same position under the bedding (5 cm
320 in depth) at one side of the test cage (31 × 25 × 12.5 cm). The time taken by the
321 mouse to retrieve the food pellet was recorded. The 3rd trial was conducted without a
322 food pellet, and the investigation time in each area during the 2 min test was measured.
323 To explore the effect of the background odorant on olfactory detection ability, a food
324 finding behavior test was performed in the presence of a food-unrelated odorant, amyl
325 acetate. Undiluted amyl acetate (100 μl; Nacalai Tesque, Kyoto, Japan) was poured
326 onto filter paper in a polystyrene dish (100 × 20 mm) with a multi-perforated lid and
327 placed on the bedding in the middle of the cage, and then the food finding behavior test
328 was performed as described above.
329
330 ***Olfactory habituation-dishabituation test.*** To evaluate the threshold of odor detection,
331 an olfactory habituation-dishabituation test was performed using an olfactometer
332 (Matsumi Group, Tokyo, Japan) to regulate the gas flow (0.5 L/min) and switch flow
333 between clean air and air with an odor, which was achieved by passing the air through a
334 bottle containing eugenol (Nacalai Tesque, Kyoto, Japan). The olfactometer,
335 connected to the test cage (31 × 25 × 12.5 cm), supplied either the clean air or the odor
336 through the gas port (0.5 mm diameter hole) on the wall (2 cm height). This test was
337 performed under the weak-light condition (<5 lux). First, the clean air was supplied to
338 the test cage, to which mice had been habituated for 15 min. In the 1st trial, mice were

continuously exposed to the air for 3 min. In the 2nd trial, the air flow was switched, and the mice were exposed to the odor for 3 min. Investigation times in the 1st and 2nd trials were measured during the 3 min test. "Investigation time" was defined as the time when the nose entered the 2.5 cm^2 square area near the gas port.

Odor-discrimination learning test. An odor-discrimination learning test was performed with 6–10-week-old (P42–P70) wild-type and *5T4* KO mice, as described previously (Imayoshi et al., 2008; Yoshihara et al., 2014) with some modifications (**Fig. 4*A***). Briefly, mice were food-restricted to maintain 80% of their free feeding weights and trained for 6 days (Day 1–6) to associate one of two odorants (odor A and odor B) with a sugar reward. During the training, the odorant was set in a polystyrene dish (100 × 20 mm) with a multi-perforated lid and placed on the bedding in the middle of the cage (26 × 40 × 18 cm). Several pieces of crystal sugar were put on the lid of the dish containing the rewarded odorant. Mice performed four 10 min trials per day: two trials for odor A paired with the sugar reward, and two trials for odor B unpaired with the sugar reward. On Days 5–7, mice received three different tests: on Day 5, the two test odorants in the dish were placed separately under the bedding (5 cm depth) without sugar on each side of the cage (26 × 40 × 18 cm); on Days 6 and 7, only one test odorant was placed under the bedding without sugar on one side of the cage (Day 6 odor A; Day 7 odor B). Behaviors were recorded with a digital video camera to measure the time (s) spent by mice in digging for each odorant during the 5 min test. On Days 5 and 6, mice were trained after receiving the above tests. The following odorants (20 μl each) were used: odor pair #1; eugenol (6.3 M) and pentanol (9.2 M)

362 (Nacalai Tesque), odor pair #2; (+) carvone (6.4 M) and (-) carvone (6.4 M) (Tokyo
363 Chemical Industry, Tokyo, Japan).
364
365 ***Object recognition test.*** To evaluate recognition memory, an object recognition test
366 was performed as described previously (Breton-Provencher et al., 2009; Bevins et al.,
367 2006). First, mice were familiarized with the test cage (31 × 25 × 12.5 cm) for 10 min
368 and returned to their home cage. One hour later, in the habituation phase, two identical
369 objects (object A; metal nut) were placed on both sides of the test cage. The time
370 spent exploring each object was recorded for 10 min. We considered the animal to be
371 exploring when its mouth, nose, or paws were in direct contact with the object. Then,
372 the mice were returned to their home cage. One hour later, in the test phase, two
373 different objects were presented: the familiar object (object A) and a novel object
374 (object B; metal bolt). The time exploring each object was recorded for 5 min. The
375 two objects with distinct features are easily distinguishable from each other by
376 non-olfactory cues such as vision and touch.
377
378 ***Olfactory avoidance test.*** An olfactory avoidance test was performed as described
379 previously (Kobayakawa et al., 2007; Kaneko-Goto et al., 2013) with some
380 modifications. To habituate the mice to the experimental environment, individual mice
381 were placed in a cage (31 × 25 × 12.5 cm) that was identical to that of the test cage for
382 30 min and then transferred to a new cage. This was repeated four times for each
383 animal. In the trial, mice were transferred to the test cage, into which a filter paper (2
384 × 2 cm) scented with three different amounts (0, 4, and 40 μl) of non-dehydrogenated
385 2,4,5-trimethylthiazole (nTMT; Tokyo Chemical Industry, Tokyo, Japan) was

386 introduced. This test was performed under the weak-light condition (<5 lux). Both
387 freezing and avoidance times were measured during the 10 min test. "Freezing time"
388 was defined as the time the mice kept still for more than 3 seconds, except for breathing.
389 "Avoidance time" was defined as the time spent in an area without a filter paper scented
390 with nTMT, when the test cage was divided into two equal areas. Avoidance behavior
391 was represented by an avoidance index (avoidance index = (P – 50)/50, where P is the
392 percentage of avoidance time during the 10 min test period).
393
394 ***Statistical analyses.*** A branching point of dendrites is the point where a neurite
395 extends from the cell body or from another neurite. A branching number of dendrites
396 is the sum of every branching point in a single neuron. All numerical data were
397 analyzed with Microsoft Excel (Microsoft, USA) with the add-in software
398 Ekuseru-Toukei 2008 (Social Survey Research Information, Tokyo, Japan).
399 Descriptive statistics were displayed as mean ± s.e.m. Student's *t* test and
400 Mann-Whitney ranked-sum test were used for pairwise comparison. Unless otherwise
401 noted, statistical significance for multiple pairwise comparisons was assessed by a
402 one-way or two-way analysis of variance (ANOVA), in which homogeneity of variance
403 was verified by Levene's test. Significant ANOVA results were subjected to Tukey's
404 multiple comparison test. Differences were deemed significant when $p < 0.05$.
405 Behavior tests such as the food finding test, habituation-dishabituation test, and
406 olfactory avoidance test, were assessed using non-parametric statistical analysis, as
407 underlying normal distribution and/or variance homogeneity could not be assumed for
408 all the samples. Multiple pairwise comparisons were carried out by Welch *t* test and
409 the resulting P-values are shown. P-values were then sequentially evaluated according

410 to the Holm–Bonferroni method (Holm, 1979) to keep an experiment-wise $\alpha \leq 0.05$.

411

412

Results

5T4 regulates the dendritic arborization of OB GCs in a cell-autonomous manner

We previously found that 5T4 regulates dendritic arborization in a specific subtype of OB GCs depending on odor experience (Yoshihara et al., 2012). We injected a lentiviral vector carrying *5T4p—gapEYFP* into the LVs of wild-type and *5T4*$^{-/-}$ mice at P3. This confirmed that *5T4*-expressing GCs, termed 5T4 GCs, are a particular subtype of interneuron, whose cell bodies are located in the MC and superficial GC layers (**Fig. 1*A***). Because 5T4 is a transmembrane protein with a leucine-rich repeat extracellular domain, we assumed that it might regulate the morphology of not only 5T4 GCs, but also that of surrounding GCs. We analyzed non-5T4 GCs that did not originate from endogenous 5T4 GCs in *5T4* KO mice. A lentiviral vector carrying *CMVp—gapEYFP* was injected into the LVs of wild-type and *5T4*$^{-/-}$ mice at P3. At P21, the non-5T4 GCs in the superficial GC and MC layers were identified by performing IHC with the 5T4 antibody in wild-type mice, and with the LacZ antibody in *5T4*$^{-/-}$ mice, in which the 5T4 coding region was replaced by *LacZ* (Southgate et al., 2010; **Fig. 1*B***). In *5T4*$^{-/-}$ mice, dendrites of LacZ-negative GCs (non-5T4 GCs) had the same branching number as those of non-5T4 GCs in wild-type mice (**Fig. 1*B***). By contrast, in *5T4*$^{-/-}$ mice, dendrites of LacZ-positive GCs (5T4 GCs) had a smaller branching number than those of 5T4 GCs in wild-type mice (**Fig. 1*A***). This result indicates that 5T4 regulates the dendritic arborization of 5T4 GCs in a cell-autonomous manner, but not that of non-5T4 GCs.

Furthermore, in the *5T4*$^{-/-}$ OB, we investigated the morphology of projection neurons that form synapses with 5T4 GCs, which exclusively overlap GAD67-positive interneurons (Imamura et al., 2006; Yoshihara et al., 2012). IHC of OB sections

showed that the loss of *5T4* did not affect the dendritic pattern of any projection neurons such as TCs (CCK-positive) and MCs (PGP9.5-positive) (**Fig. 2*B***), consistent with the results of Golgi-Cox staining showing no changes in the morphology of ETCs and MCs (**Fig. 2*C***). These results demonstrate that 5T4 specifies the dendritic branching of 5T4 GCs, but not that of their synaptic partners, ETCs and MCs. We also confirmed that the loss of *5T4* did not affect the number of 5T4 GCs (**Fig. 2*A***).

Notably, BrdU labeling of newborn neurons revealed that 5T4 GCs were generated predominantly during the embryonic (E15.5) and neonatal (P0) stages, rather than during the infant (P14) and young stages (P28) (**Fig. 1*C***). This suggested that 5T4 GCs, located in the MC and superficial GC layers, have a lower turnover rate than other GCs in the deep layer (**Fig. 1*A***). This is supported by previous reports showing that newborn OB interneurons at the adult stage are replaced preferentially by old ones in the deep GC layer (Sakamoto et al., 2014; Imayoshi et al., 2008).

Electrophysiological recordings of acute OB slices classify ETCs into two types

Because 5T4 GCs arborize their dendrites into the EPL where ETCs elongate their lateral dendrites (Mori et al., 1983; Orona et al., 1984), we assumed that 5T4 GCs would form dendrodendritic synapses preferentially with ETCs (Imamura et al., 2006). Previous studies show that a distinct subpopulation of ETCs have distinct electrophysiological properties and different dendritic branching patterns (Antal et al., 2006; Macrides and Schneider, 1982). To elucidate the relationship between 5T4 GCs and ETCs, we first characterized the electrophysiological properties of ETCs in acute OB slices from wild-type mice. Interestingly, cell-attached recordings revealed that there are at least two types of ETCs: one type showing periodic bursts of spontaneous

462 firings and another type showing lower spontaneous firing rates than the first type (**Fig.**
463 **3*A***). Based on current-clamp recordings, we defined ETCs with or without a rebound
464 burst firing after the current pulse as bursting or non-bursting ETCs, respectively (Antal
465 et al., 2006; **Fig. 3*C*** (asterisk)**, *E***). According to this definition, bursting ETCs in
466 wild-type mice also had a more prominent sag during hyperpolarizing current injection,
467 compared with non-bursting ETCs (**p < 0.0001; bursting ETC, n = 17 cells from ten
468 animals; non-bursting ETC, n = 20 cells from eleven animals; **Fig. 3*C*** (arrow)**, *E*, *F***), as
469 reported previously in the rat OB (Antal et al., 2006). After the electrophysiological
470 recordings, ETC dendrites were visualized by injecting biocytin. Interestingly, there
471 was a remarkable difference in dendrite morphology between bursting and non-bursting
472 ETCs: non-bursting ETCs had basal dendrites extending laterally into the superficial
473 EPL (**Fig. 3*D***), whereas bursting ETCs had not (**Fig. 3*B***).
474 Next, we investigated the electrophysiological properties of ETCs in the *5T4* KO
475 mice. As in the case of wild-type mice, bursting ETCs showed a significantly higher
476 sag ratio than non-bursting ETCs in *5T4* KO mice (**p < 0.0001; bursting ETC, n = 17
477 cells from nine animals; non-bursting ETC, n = 19 cells from nine animals; **Fig. 3*F***).
478 There was no significant difference in the sag ratio between wild-type and *5T4* KO mice
479 (**Fig. 3*F***). These results suggest that the impaired dendritic development of 5T4 GCs
480 does not affect the development of the two ETC types *per se* in *5T4* KO mice, which is
481 consistent with the IHC data for *5T4*$^{-/-}$ OBs (**Fig. 2*B, C***).
482
483 **Optogenetic stimulation of *ChR2*-expressing 5T4 GCs in OB slices**
484 Then, we utilized optogenetics to examine which types of projection neurons would
485 form synapses with 5T4 GCs. To induce the expression of the *ChR2-EYFP* gene in

5T4 GCs, a lentivirus expressing the *Cre* gene under the control of the *5T4* promoter (*5T4p—Cre*) was injected into both LVs and OBs of Ai32 (*Rosa26—ChR2-EYFP*) mice (Madisen et al., 2012) at P1. After 3 weeks, we observed that 73% of ChR2-EYFP$^+$ cells were 5T4 GCs, whereas 9% of 5T4 GCs expressed *ChR2-EYFP* (n = 4 sections from two animals; **Fig. 4*A, B***). To activate 5T4 GC dendrites, we light-stimulated the superficial, upper half of the EPL in acute OB slices from *ChR2-EYFP*-expressing Ai32 mice, and measured light-evoked $GABA_A$-PSCs in an individual ETC (**Fig. 4*C***). Remarkably, light stimulation of 5T4 GCs induced a $GABA_A$-PSC in a non-bursting ETC; however, the induction of $GABA_A$-PSC was inhibited entirely by adding a $GABA_A$ receptor antagonist, SR95531 (**Fig. 4*D***). Consistent with 9% of 5T4 GCs expressing *ChR2* (**Fig. 4*B***), 7% of non-bursting ETCs displayed optogenetically-evoked PSCs (**Fig. 4*E***). These results indicate that 5T4 GCs form GABAergic synapses with non-bursting ETCs. Furthermore, light stimulation of 5T4 GCs also induced a $GABA_A$-PSC in a bursting ETC and an MC (**Fig. 4*E***). The mean amplitude of $GABA_A$-PSCs was indistinguishable among the bursting ETC, non-bursting ETC and MC (**Fig. 4*F***). These results suggest that 5T4 GC dendrites form GABAergic synapses with not only non-bursting ETCs, but also bursting ETCs and MCs to regulate neural activity.

Inhibitory synaptic inputs onto non-bursting ETCs are significantly lower in *5T4* KO mice than in wild-type mice

Because 5T4 GCs form inhibitory synapses with the two types of ETCs and the MCs (**Fig. 4**), we assumed that the impaired dendritic development of 5T4 GCs in *5T4* KO mice would exclusively affect GC-derived $GABA_A$-PSCs in the projection neurons.

To examine this assumption, we first stimulated the EPL in OB slices with a bipolar platinum electrode and measured electrically evoked $GABA_A$-PSCs in the two types of ETCs (**Fig. 5*B left***). To block AMPA/KA receptor-mediated currents, CNQX (10 μM) was added to ACSF. Electrical stimulation of the EPL induced distinctive $GABA_A$-PSCs in non-bursting ETCs within the wild-type OB (**Fig. 5*C***). Interestingly, even when the electrical stimulation in the EPL was increased from the threshold by typically 10 μA, the amplitude of the $GABA_A$-PSCs increased only a little (**Fig. 5*C, E***). In addition, a representative trace of evoked $GABA_A$-PSCs showed a small fall time (**Fig. 5*C***) and resembled closely that of spontaneous $GABA_A$-PSCs (**Fig. 5*A***). These results indicated that electrically evoked $GABA_A$-PSCs in non-bursting ETCs were elicited by activation of a few GCs, presumably involving one neuron with processes within the stimulated area under our experimental conditions. Similar results were obtained in bursting ETCs from the wild-type OB (**Fig. 5*D***).

Since our data suggest that GC dendrites connecting to a single ETC are sparsely distributed in the OB EPL, we investigated GABAergic inputs from a single GC to individual ETCs. We defined $GABA_A$-PSCs induced by stimulation with a current 2–4 μA larger than the threshold as the stable-minimal response for the ETCs, because the current intensity at the threshold sometimes failed to evoke the $GABA_A$-PSC in individual ETCs (**Fig. 5*C***; 12 μA). We used 20 traces including failures in each current intensity (total 40 traces) to calculate the amplitude of $GABA_A$-PSC in individual cells and compared the amplitudes between wild-type and *5T4*$^{-/-}$ OBs. In bursting ETCs, there was no significant difference in the amplitude of $GABA_A$-PSCs between wild-type and *5T4* KO OBs (**Fig. 5*G***). Conversely, in non-bursting ETCs, the median amplitude of $GABA_A$-PSCs was 29% lower in *5T4* KO than in wild-type OBs

534 ($p < 0.01$ [Mann-Whitney rank-sum test]; WT, n = 22; *5T4* KO, n=21; **Fig. 5*H***).
535 Furthermore, the electrically-evoked PSC charge through integration of the waveform
536 for 50 ms in non-bursting ETCs was also significantly larger in the wild-type OB than
537 in the *5T4*$^{-/-}$ OB ($p < 0.05$ [Mann-Whitney rank-sum test]; WT, n = 22; *5T4* KO, n=21;
538 **Fig. 5*H***). These results suggest that the impaired dendritic development of 5T4 GCs
539 in *5T4* KO mice leads to reduced GABAergic inputs into non-bursting ETCs, but not
540 into bursting ETCs. Furthermore, we stimulated the superficial GC layer in OB slices
541 with a bipolar platinum electrode and measured evoked $GABA_A$-PSCs in an MC (**Fig.**
542 **5*B right, F***). In MCs, there was no significant difference in the amplitude of
543 $GABA_A$-PSCs between wild-type and *5T4* KO OBs (**Fig. 5*I***).
544 Notably, in the wild-type OB, non-bursting ETCs showed a 60% larger amplitude
545 of $GABA_A$-PSCs and a 44% lower coefficient of variation than bursting ETCs (in
546 median value; **Fig. 5*G, H***). It is reported that an increase in the number of synaptic
547 release sites leads to a decrease in the coefficient of variation for the synaptic response
548 amplitude (Faber and Korn, 1991). These results reveal that non-bursting ETCs form
549 more inhibitory synapses with GCs including 5T4 GCs than bursting ETCs in the
550 wild-type OB, and thus are more affected by the impaired dendritic development of 5T4
551 GCs than bursting ETCs in the *5T4* KO OB.
552 GCs form bidirectional dendrodendritic synapses with projection neurons in the
553 OB (Shepherd et al., 2004). Thus, in addition to recording inhibitory postsynaptic
554 transmission onto ETCs, we explored postsynaptic transmission in the opposite
555 direction, namely, EPSCs onto 5T4-derived GCs in OB slices of wild-type and *5T4* KO
556 mice (**Fig. 6*A–C***). Electrical stimulation of the EPL induced distinctive EPSCs in the
557 5T4 GCs within wild-type OB slices (**Fig. 6*D***). Intriguingly, we found that

5T4-derived GCs received significantly fewer glutamatergic inputs in *5T4* KO than in wild-type OBs (**Fig. 6*E***). The median amplitude of EPSCs in 5T4 GCs was 50% lower in *5T4* KO than in wild-type OBs ($p = 0.0077$ [Mann-Whitney rank-sum test]; **Fig. 6*E***). These results strongly suggest that a combination of reduced inhibitory transmission onto non-bursting ETCs and reduced excitatory transmission onto 5T4 GCs might cause some kind of behavioral change in *5T4* KO mice.

Detection thresholds for odors are higher in *5T4* KO mice

Because *5T4* KO mice showed significant reductions both in dendrite branching of 5T4 GCs (**Fig. 1*A***) and in synaptic transmission onto ETCs and 5T4 GCs (**Figs. 5 and 6**), we conducted a behavior test to assess olfactory detection in these mice. *5T4* KO mice were born normally, and showed no obvious abnormalities in mating, nursing, or feeding behavior. Since adult *5T4*$^{-/-}$ mice exhibit a high frequency of hydrocephalus (approximately 13%; Southgate et al., 2010), we used 6–10-week-old male mice (P42–P70) without hydrocephalus in the following experiments. First, using a food finding test (Le Pichon et al., 2009), we measured the time taken by the fasted mice to find a food pellet hidden under the bedding on one side of the cage. In the 1st trial, mice retrieving food faster than other mice were assumed to have a better sense of smell. However, there was no difference between wild-type and *5T4* KO mice with respect to the time taken to find food in the 1st trial (**Fig. 7*A***). This result indicated that *5T4* KO mice could detect the smell of food as well as wild-type mice. In the 2nd trial with the food pellet buried in the same place as in the 1st trial, there was no difference in the times taken to find the food between wild-type and *5T4* KO mice (**Fig. 7*A***). To study the spatial memory of *5T4* KO mice, we performed the 3rd trial without the food pellet

582 and measured the time the mice spent in each side of the cage. Both wild-type and
583 *5T4* KO mice spent significantly more time near the area where the food pellet had been
584 buried in the 1st and 2nd trials (**Fig. 7*A***). These results suggest that *5T4* KO mice can
585 learn and memorize the position of food as well as wild-type mice.
586 Next, we used a habituation-dishabituation test to examine odor-detection
587 thresholds. Mice were exposed to clean air using an olfactometer and were then
588 provided with air in the 1st trial. Because the mice had been habituated to clean air,
589 the investigation time was shorter in this trial (**Fig. 7*B***). In the 2nd trial, a test odorant,
590 eugenol, at four different concentrations (0.63, 6.3, 63, and 630 μM) was presented to
591 the mice. Differences in investigation times between 1st and 2nd trials were analyzed
592 in wild-type and *5T4* KO mice. At 6.3 and 63 μM, the investigation time of *5T4* KO
593 mice was remarkably shorter than that of wild-type mice ($p < 0.01$ and 0.05,
594 respectively; $n = 5$ animals in each condition; **Fig. 7*B***), while at 630 μM, the
595 investigation time of *5T4* KO mice was similar to that of wild-type mice (**Fig. 7*B***).
596 These results suggest that the odor-detection thresholds of *5T4* KO mice are more than
597 100-fold higher than those of wild-type mice.
598 Furthermore, we performed an olfactory avoidance test (Kobayakawa et al., 2007;
599 Kaneko-Goto et al., 2013). A component of fox feces, TMT (2,4,5-trimethylthiazole),
600 evokes innate fear responses in rodents (Vernet-Maury et al., 1984; Fendt et al., 2005).
601 We found that nTMT also induced similar freezing and avoidance responses between
602 wild-type and *5T4* KO mice when a high amount (40 μl) of nTMT was used (**Fig. 7*C***).
603 Interestingly, when a lower amount (4 μl) of nTMT was employed, wild-type mice
604 showed significant freezing and avoidance responses, compared with *5T4* KO mice
605 (freezing, 20%; avoidance, 69%; $p < 0.01$, 0.05, respectively; $n = 5$; **Fig. 7*C***). These

606 results strongly suggest that detection sensibility for odors is impaired in *5T4* KO mice,
607 which is consistent with the results in **Fig. 7*B***.
608 However, the results of the habituation-dishabituation test could have been affected
609 by differences in the exploratory behaviors of the mice. Because *5T4* is expressed in
610 other brain regions, including eye, neocortex, amygdala, and inferior colliculus
611 (Imamura et al., 2006; our unpublished data), we performed a novel object recognition
612 test (**Fig. 7*D***) to assess recognition memory and incentive-directed motivation in global
613 *5T4* KO mice (Breton-Provencher et al., 2009; Bevins et al., 2006). After habituating
614 the mice to an object, the mice were exposed to a novel object, and the time taken by the
615 mice to explore the object was measured. Although both wild-type and *5T4* KO mice
616 spent more time exploring the novel object than the familiar one, there was no
617 significant difference between the two mice (**Fig. 7*D***). Therefore, these results
618 confirm that exploratory behavior for object recognition was unaffected in *5T4* KO
619 mice.
620
621 **Odor-discrimination learning is impaired in *5T4* KO mice**
622 We explored whether dendritic development in OB GCs would be required for
623 odor-discrimination learning and memory (Imayoshi et al., 2008). We compared the
624 performances of wild-type and *5T4* KO mice at 6–10 weeks old (P42–P70) in an
625 odor-discrimination learning test using two undiluted odorants. Mice were trained for
626 Day 1–4 to associate an odorant, eugenol, with a sugar reward (**Fig. 8*A***). During the
627 training, *5T4* KO mice consumed sugar at a similar level to that of wild-type mice
628 (wild-type = 0.15 ± 0.01 g/day; *5T4* KO = 0.13 ± 0.01 g/day; $p > 0.05$; n = 8 animals
629 from each line; **Fig. 8*A***). On Day 5 (Test 1), we placed two odorants, eugenol and

630 pentanol, separately underneath the bedding without any sugar, and measured the time
631 the mice spent digging near each odor. Wild-type mice spent significantly more time
632 digging near eugenol than near pentanol ($p < 0.05$; $n = 5$; **Fig. 8*B***), while *5T4* KO mice
633 spent nearly the same time digging for eugenol and pentanol (**Fig. 8*B***). These results
634 indicate that loss of *5T4* impairs odor-discrimination learning.
635 Because the odor-detection thresholds were remarkably higher in *5T4* KO mice
636 (**Fig. 7*B, C***), it was uncertain whether these mice could detect odorants buried under the
637 cage bedding in Test 1. To address this issue, we performed additional tests using
638 eugenol and pentanol on Day 6 (Test 2) and Day 7 (Test 3), respectively. Interestingly,
639 in Test 2, *5T4* KO mice spent significantly more time digging near the area scented with
640 eugenol (associated with the sugar reward) than in the opposite area, as in the case of
641 wild-type mice ($p < 0.05$; $n = 5$ animals from each line; **Fig. 8*B***). By contrast, in Test
642 3, neither wild-type nor *5T4* KO mice preferred to dig near the area scented with
643 pentanol (not associated with the sugar reward) (**Fig. 8*B***). These results suggested that
644 *5T4* KO mice could learn that eugenol was the odor associated with sugar during the
645 training phase, and detect eugenol buried under the cage bedding in Test 2. However,
646 *5T4* KO mice could not discriminate eugenol when both odors were present in Test 1,
647 whereas wild-type mice could. Similar results were obtained in another
648 odor-discrimination learning test using a pair of structurally related odors, (+) carvone
649 and (-) carvone (**Fig. 8*C***). These results strongly suggest that 5T4-dependent dendritic
650 development of OB GCs is required for discriminating between two different odors.
651 To further support this conjecture, we investigated the ability of the mice to
652 discriminate an odor of interest in the presence of a background unrelated odor.
653 Notably, exposure to a high concentration of amyl acetate induced the expression of

654 *cFos* (a marker of neuronal activity) in 38% of 5T4 GCs (**Fig. 9*A, B***). This suggested
655 that the odor signal from amyl acetate was processed by 5T4 GCs in the broad area of
656 the OB, consistent with our previous data (Yoshihara et al., 2014). There was no
657 significant difference between wild-type and *5T4* KO mice in a normal food finding test
658 without a food-unrelated odorant such as amyl acetate (**Fig. 7*A***). By contrast, in a
659 food finding test with amyl acetate, *5T4* KO mice needed more time to find a food pellet
660 in the 1st trial than wild-type mice (**Fig. 9*C***), while there was no significant difference
661 between both mice in the 2nd and 3rd trials (**Fig. 9*C***). These results clearly revealed
662 that *5T4* KO mice cannot discriminate an odor of interest from a background odor.
663
664 **Olfactory behaviors are also impaired in OB-specific *5T4* KD mice**
665 Although global *5T4* KO mice showed impaired olfactory behaviors (**Figs. 7–9**), it was
666 unclear whether these phenotypes were due to defects in the dendritic development of
667 5T4 GCs in the OB alone. Thus, we performed an OB-specific *5T4* KD experiment
668 with three lentiviral vectors expressing different *5T4-shRNAs* under the control of the
669 human *H1* promoter (*H1p—5T4-shRNAs*), as described previously (Yoshihara et al.,
670 2012). Lentiviral vectors carrying three kinds of *H1p—5T4-shRNAs* were injected
671 into both the LVs and OBs of wild-type mice at P1, where they infected LV neural stem
672 cells and OB cells such as interneurons and projection neurons. Because *5T4*
673 expression was restricted predominantly to the GAD67-positive interneurons in the OB
674 (Imamura et al., 2006; Yoshihara et al., 2012), *5T4* KD appeared to be specific to 5T4
675 GCs in the OB. In fact, IHC of OB sections with the 5T4 antibody indicated that the
676 amount of 5T4 in the dendrites of 5T4 GCs within the EPL was 29% lower in *5T4* KD
677 mice than in control mice, into which three kinds of *H1p—scramble-shRNAs* had been

678 injected (**Fig. 10*A***).

679 Next, we conducted an olfactory behavior test with 6–10-week-old OB-specific
680 *5T4* KD mice (P42–70). In the habituation-dishabituation test, the investigation time
681 of *5T4* KD mice was remarkably shorter than that of control mice in Test 1 using
682 eugenol at 6.3 μM ($p < 0.05$; $n = 5$ animals in each condition; **Fig. 10*B***), while in Test 2
683 with 630 μM eugenol, the investigation time of *5T4* KD mice was similar to that of the
684 control mice (**Fig. 10*B***). Furthermore, in the olfactory avoidance test using the lower
685 amount (4 μl) of nTMT, the *5T4* KD mice showed fewer freezing responses than the
686 control mice (43%; $p < 0.05$, respectively; $n = 5$ animals in each condition; **Fig. 10*C***).
687 These results revealed that odor-detection thresholds are higher in OB-specific *5T4* KD
688 mice as well as in global *5T4* KO mice (**Fig. 7*B, C***).

689 In the odor-discrimination learning test with both eugenol and pentanol, *5T4* KD
690 mice did not spend significantly more time digging near the area scented with eugenol
691 (associated with the sugar reward) than near the area scented with pentanol (not
692 associated with the sugar reward) (**Fig. 10*D***). This revealed that *5T4* KD mice could
693 not discriminate eugenol when both odors were present in Test 1. The OB-specific
694 *5T4* KD showed the same defect as the global *5T4* KO in these olfactory behavior tests
695 (**Figs. 7*B, C* and 8*B***), further suggesting that 5T4 GCs in the OB are required for both
696 odor-detection and -discrimination behaviors.

697

Discussion

The neural circuitry between 5T4 GCs and non-bursting ETCs

ETCs appear to be glutamatergic projection neurons located either in the glomerular layer or at the superficial border of the EPL. In this study, we found that mouse ETCs can be divided into two types, bursting and non-bursting (**Fig. 3**), as shown previously for the rat OB (Antal et al., 2006). Recent studies in the rat revealed the characteristic properties of ETCs, especially bursting ETCs, which are defined by their spontaneous periodic burst firings in OB slices and lack of basal dendrites (Antal et al., 2006; Hayar et al., 2004a; Liu and Shipley, 2008). The bursting ETCs modulate the input pattern from olfactory sensory neurons with their intrinsic membrane properties and provide the feed-forward excitatory output to MCs (De Saint Jan et al., 2009; Gire et al., 2012). Moreover, bursting ETCs provide monosynaptic glutamatergic input to and receive GABAergic feedback from PGCs and SACs (Hayer et al., 2004b; Banerjee et al., 2015). Thus, the bursting ETC is believed to function as a central unit for the processing of olfactory signals within a glomerulus. Interestingly, we observed the optogenetically- and electrically-evoked $GABA_A$-PSCs in bursting ETCs (**Figs. 4 and 5**). Our results suggest that GCs may form GABAergic synapses with the cell bodies of bursting ETCs located in the glomerular layer near the EPL border. However, we cannot exclude the possibility that optogenetically-evoked $GABA_A$-PSC events in bursting ETCs reflect *5T4*-expressing PGCs (5T4 PGCs), if any, a small fraction of PGCs (Yoshihara et al., 2012).

Compared with the information available for bursting ETCs, we know relatively little about non-bursting ETCs. Although optogenetic stimulation suggested that 5T4

GCs connect to both non-bursting and bursting ETCs (**Fig. 4**), electrical stimulation showed that *5T4* KO mice have fewer inhibitory inputs from GCs to non-bursting ETCs than those from GCs to bursting ETCs (**Fig. 5**). In addition, electrical stimulation suggested that GC dendrites connecting to a single non-bursting ETC are sparsely distributed in the EPL (**Fig. 5**), as reported previously for the dendrodendritic interactions between MCs and GCs (Fantana et al., 2008; Kato et al., 2013; Kim et al., 2011). The sparse, rather than dense, interactions between GCs and MCs/TCs, including non-bursting ETCs, suggest that the EPL is a lateral inhibitory network in the OB, unlike the nearest-neighbor lateral inhibitory systems in the other modalities such as the retina, which depend on dense interactions (Cook and McReynolds, 1998; Cleland et al., 2014). Interestingly, optogenetic analysis revealed that a small fraction (9%) of *ChR2*-expressing 5T4 GCs induce light-evoked $GABA_A$-PSCs in 7% of non-bursting ETCs (**Fig. 4**). Therefore, we assume that a single non-bursting ETC can usually receive inhibitory input from at least one 5T4 GC. Our results indicate that, among several subtypes of OB GCs, a specific 5T4 GC subtype plays an important role in regulating neural activity in non-bursting ETCs. Furthermore, 5T4 GCs received fewer glutamatergic inputs in *5T4* KO than in wild-type OBs (**Fig. 6**). Taken together, these results suggest that the changes in excitatory and inhibitory transmission involving 5T4 GCs account for the dysfunctional behavior (**Figs. 7–10**). However, we cannot exclude the possibility that *5T4* KO and KD effects on the behavior are explained by the effects of not only 5T4 GCs but also 5T4 PGCs on the neural circuity.

How does the impaired dendritic development in 5T4 GCs influence odor-detection thresholds?

5T4 KO mice showed impaired odor detection in thresholds (**Fig. 7**). Because we could not obtain any evidence that loss of *5T4* affects the morphologies of MCs/TCs or the intrinsic membrane properties of ETCs (**Figs. 2 and 3**), it is unlikely that the loss of *5T4* reduces the excitability of MCs/TCs. One possible explanation for elevated odor-detection thresholds in *5T4* KO mice is that the impaired dendritic development of 5T4 GCs may disturb oscillatory neuronal activities in the OB. The synchronized firing of MCs/TCs induces prominent γ-range oscillations in the local field potential, which is necessary for effective transmission of the odor signal to the olfactory cortex during awake behaving states (Manabe and Mori, 2013). Dendrodendritic reciprocal synapses between MCs/TCs and GCs participate in the generation of γ-range oscillations in the OB (Nusser et al., 2001; Lagier et al., 2004). Therefore, the reduced number of inhibitory synaptic connections between 5T4 GCs and non-bursting ETCs in the *5T4* KO mice may disturb the generation of the synchronized oscillatory firings in ETCs, and thus may hinder the transmission of olfactory signals from the OB to the olfactory cortex, resulting in poor odor detection ability (**Fig. 7**).

How does impaired dendritic development in 5T4 GCs influence odor-discrimination learning?

OB GCs mediate inhibitory interactions with MCs/TCs, which provide lateral and recurrent inhibitions. When mice sniff an object, the odor information is transformed into a spatial pattern of activated glomeruli in the OB (Mori and Sakano, 2011). The lateral inhibition between GCs and MCs/TCs appears to enhance the contrast between strongly and weakly activated glomeruli, and thus sharpens the tuning specificity of individual MCs/TCs to odor molecules (Kato et al., 2012; Yokoi et al., 1995). GCs

modulate the activity of MCs/TCs including non-bursting ETCs via sparse interactions in the EPL rather than via nearest-neighbor lateral inhibition (Fantana et al., 2008; Kato et al., 2013; Kim et al., 2011; **Fig. 5**). We previously reported that 5T4 GCs have higher branching dendrites than non-5T4 GCs (Yoshihara et al., 2012; **Fig. 1**). Furthermore, non-bursting ETCs broadly elongate their lateral dendrites in the EPL (Igarashi et al., 2012; **Fig. 3**). Thus, we speculate that 5T4 GC dendrites may broadly and efficiently regulate the neural activity of non-bursting ETCs in an odor experience-dependent manner. Further, the impaired dendritic development of endogenous 5T4 GCs in *5T4* KO mice may result in a failure to reshape neural circuits that execute the unmasking and filtering functions required to discriminate between two odors (**Fig. 8**). This interpretation is supported by the observation that *5T4* KO mice cannot discriminate an odor of interest from a background odor in the food finding test (**Fig. 9**).

Interestingly, the results for the olfactory behavior task with *5T4* KO mice differ from those reported in other studies, in which either inhibition or activation of neural activity in the adult-born OB interneurons did not have any remarkable effect on either odor-detection thresholds or the performance of simple odor-discrimination tasks (Abraham et al., 2010; Alonso et al., 2012; Sakamoto et al., 2014). This discrepancy could be due to a difference in subtypes of OB interneurons genetically manipulated in each study. Because GCs can be divided into several subtypes based on their morphology (Merkle et al., 2014), it is assumed that each GC subtype forms a distinct local circuit in the OB (Mori et al., 1983; Orona et al., 1983; Shepherd et al., 2004). Several subtypes of GCs are derived from distinct neural stem cells in the SVZ (Fuentealba et al., 2015). Manipulated adult-born GCs are integrated predominantly

794 into deep regions of the OB GC layer, and tend to interact with MCs rather than with
795 TCs (Bardy et al., 2010; Sakamoto et al., 2014). By contrast, 5T4 GCs are located in
796 the MC and superficial GC layers, and are generated mainly during the embryonic and
797 neonatal stages, rather than during the young adult stage (**Fig. 1**). It is likely that
798 embryonic-born OB interneurons, including 5T4 GCs, play a fundamental role in innate
799 olfactory responses for survival, such as predator-avoidance and suckling behaviors
800 (**Figs. 7–10**), whereas adult-born OB interneurons are required for learned olfactory
801 behaviors (Alonso et al., 2012; Sakamoto et al., 2014). A recent study reported that
802 local dendrodendritic circuits within the EPL may segregate into parallel MC and TC
803 (ETC) pathways (Fourcaud-Trocmé et al., 2014). Interestingly, Igarashi et al. (2012)
804 reported that TCs have odor-induced firing responses with shorter latencies at lower
805 concentration thresholds than those of MCs. TCs (ETCs) may be specialized in the
806 fast odor detection and fast behavioral responses that are required for simple
807 discrimination between two distinctly different odors, whereas MCs may be specialized
808 in performing the more difficult task of discriminating between two closely related
809 odors such as enantiomers. This conjecture is consistent with the higher
810 odor-detection thresholds of the *5T4* KO mice and their impaired aptitude in
811 odor-discrimination learning between two quit e different odors, eugenol and pentanol
812 (**Figs. 7 and 8**). Since the loss of *5T4* reduced GC-derived GABAergic inputs onto
813 non-bursting ETCs, but not onto MCs (**Fig. 5**), it is possible that 5T4 GCs may
814 preferentially modulate the ETC pathway to regulate both odor-detection thresholds and
815 simple odor-discrimination learning. However, because the activation of ETCs evokes
816 feed-forward excitation to MCs (De Saint Jan et al., 2009; Gire et al., 2012), we cannot
817 exclude the possibility that impaired dendritic development of 5T4 GCs in the *5T4* KO

mice may also affect the MC pathway via non-bursting ETCs. Future studies on MCs and TCs (ETCs) in *5T4* KO mice should help increase understanding of their roles in odor-associated behaviors, which are mediated by their interactions with 5T4 GCs in the OB neural circuitry.

References

Abraham NM, Egger V, Shimshek DR, Renden R, Fukunaga I, Sprengel R, Seeburg PH, Klugmann M, Margrie TW, Schaefer AT, Kuner T (2010) Synaptic inhibition in the olfactory bulb accelerates odor discrimination in mice. Neuron 65:399–411.

Adam Y, Mizrahi A (2010) Circuit formation and maintenance - perspectives from the mammalian olfactory bulb. Curr Opin Neurobiol 20:134–140.

Alonso M, Lepousez G, Sebastien W, Bardy C, Gabellec MM, Torquet N, Lledo PM (2012) Activation of adult-born neurons facilitates learning and memory. Nat Neurosci 6:897–904.

Antal M, Eyre M, Finklea B and Nusser Z (2006) External tufted cells in the main olfactory bulb form two distinct subpopulations. Eur J Neurosci 24:1124–1136.

Bardy C, Alonso M, Bouthour W, Lledo PM (2010) How, when, and where new inhibitory neurons release neurotransmitters in the adult olfactory bulb. J Neurosci 30:17023–17034.

Banerjee A, Marbach F, Anselmi1 F, Koh MS, Davis MB, da Silva PG, Delevich K, Oyibo HK, Gupta P, Li B, Albeanu DF (2015) An Interglomerular Circuit Gates Glomerular Output and Implements Gain Control in the Mouse Olfactory Bulb. Neuron 87:193–207.

Barrow KM, Ward CM, Rutter J, Ali S, Stern PL (2005) Embryonic expression of murine 5T4 oncofoetal antigen is associated with morphogenetic events at implantation and in developing epithelia. Dev Dyn 233:1535–1545.

Bevins RA, Besheer J (2006) Object recognition in rats and mice: a one-trial non-matching-to-sample learning task to study 'recognition memory'. Nat Protoc 1:1306–1311.

Breton-Provencher V, Lemasson M, Peralta MR 3rd and Saghatelyan A (2009) Interneurons produced in adulthood are required for the normal functioning of the olfactory bulb network and for the execution of selected olfactory behaviors. J Neurosci

29:15245–15257.

Cleland TA (2014) Construction of odor representations by olfactory bulb microcircuits. Prog Brain Res. 208:177–203.

Cook PB, McReynolds JS (1998) Lateral inhibition in the inner retina is important for spatial tuning of ganglion cells. Nat Neurosci 1:714–719.

De Saint Jan D, Hirnet D, Westbrook GL Charpak S (2009) External tufted cells drive the output of olfactory bulb glomeruli. J Neurosci 29:2043–2052.

Faber DS and Korn H (1991) Applicability of the coefficient of variation method for analyzing synaptic plasticity. Biophys J 60:1288–1294.

Fantana AL, Soucy ER, Meister M (2008) Rat olfactory bulb mitral cells receive sparse glomerular inputs. Neuron 59:802–814.

Fendt M, Endres T, Lowry CA, Apfelbach R, McGregor IS (2005) TMT-induced autonomic and behavioral changes and the neural basis of its processing. Neurosci Biobehav Rev 29:1145–1156.

Fourcaud-Trocmé N, Courtiol E, Buonviso N (2014) Two distinct olfactory bulb sublaminar networks involved in gamma and beta oscillation generation: a CSD study in the anesthetized rat. Front Neural Circuits 8:88.

Fuentealba LC, Rompani SB, Parraguez JI, Obernier K, Romero R, Cepko CL, Alvarez-Buylla A (2015) Embryonic Origin of Postnatal Neural Stem Cells. Cell 161:1644–1655.

Gire DH, Franks KM, Zak JD, Tanaka KF, Whitesell JD, Mulligan AA, Hen R, Schoppa NE (2012) Mitral cells in the olfactory bulb are mainly excited through a multistep signaling path. J Neurosci 32:2964–2975.

Hayar A, Karnup S, Shipley MT and Ennis M (2004a) Olfactory bulb glomeruli: external tufted cells intrinsically burst at theta frequency and are entrained by patterned olfactory input. J Neurosci 24:1190–1199.

Hayar A, Karnup S, Ennis M, Shipley MT (2004b) External tufted cells: a major excitatory element that coordinates glomerular activity. J Neurosci 24:6676–6685.

Hole N, Stern PL (1990) Isolation and characterization of 5T4, a tumour-associated antigen. Int J Cancer 45:179–184.

Holm S (1979) A simple sequentially rejective multiple test procedure. Scand J Statist 6:65–70.

Igarashi KM, Ieki N, An M, Yamaguchi Y, Nagayama S, Kobayakawa K, Kobayakawa R, Tanifuji M, Sakano H, Chen WR, Mori K (2012) Parallel mitral and tufted cell pathways route distinct odor information to different targets in the olfactory cortex. J Neurosci 32:7970–7985.

Imamura F, Nagao H, Naritsuka H, Murata Y, Taniguchi H, Mori K (2006) A leucine-rich repeat membrane protein, 5T4, is expressed by a subtype of granule cells with dendritic arbors in specific strata of the mouse olfactory bulb. J Comp Neurol 495:754–768.

Imayoshi I, Sakamoto M, Ohtsuka T, Takao K, Miyakawa T, Yamaguchi M, Mori K, Ikeda T, Itohara S, Kageyama R (2008) Roles of continuous neurogenesis in the structural and functional integrity of the adult forebrain. Nat Neurosci 11:1153–1161.

Ishii T, Omura M, Mombaerts P (2004) Protocols for two- and three-color fluorescent RNA in situ hybridization of the main and accessory olfactory epithelia in mouse. J Neurocytol 33:657–669.

Kaneko N, Marin O, Koike M, Hirota Y, Uchiyama Y, Wu JY, Lu Q, Tessier-Lavigne M, Alvarez-Buylla A, Okano H, Rubenstein JL, Sawamoto K (2010) New neurons clear the path of astrocytic processes for their rapid migration in the adult brain. Neuron 67:213–223.

Kaneko-Goto T, Sato Y, Katada S, Kinameri E, Yoshihara S, Nishiyori A, Kimura M, Fujita H, Touhara K, Reed RR, Yoshihara Y (2013) Goofy coordinates the acuity of olfactory signaling. J Neurosci 2013 33:12987–12996.

Kato HK, Chu MW, Isaacson JS, Komiyama T (2012) Dynamic sensory representations in the olfactory bulb: modulation by wakefulness and experience. Neuron 76:962–975.

Kato HK, Gillet SN, Peters AJ, Isaacson JS, Komiyama T (2013) Parvalbumin-expressing interneurons linearly control olfactory bulb output. Neuron 80:1218–1231.

Kim DH, Phillips ME, Chang AY, Patel HK, Nguyen KT, Willhite DC (2011) Lateral Connectivity in the Olfactory Bulb is Sparse and Segregated. Front Neural Circuits 5:5.

King KW, Sheppard FC, Westwater C, Stern PL, Myers KA (1999) Organisation of the mouse and human 5T4 oncofoetal leucine-rich glycoprotein genes and expression in foetal and adult murine tissues. Biochim Biophys Acta 1445: 257–270.

Kobayakawa K, Kobayakawa R, Matsumoto H, Oka Y, Imai T, Ikawa M, Okabe M, Ikeda T, Itohara S, Kikusui T, Mori K, Sakano H (2007) Innate versus learned odour processing in the mouse olfactory bulb. Nature 450:503–508.

Lagier S, Carleton A, Lledo PM (2004) Interplay between local GABAergic interneurons and relay neurons generates gamma oscillations in the rat olfactory bulb. J Neurosci 24:4382–4392.

Le Pichon CE, Valley MT, Polymenidou M, Chesler AT, Sagdullaev BT, Aguzzi A, Firestein S (2009) Olfactory behavior and physiology are disrupted in prion protein knockout mice. Nat Neurosci 12:60–69.

Lepousez G, Valley MT, Lledo PM (2013) The impact of adult neurogenesis on olfactory bulb circuits and computations. Annu Rev Physiol 75:339–363.

Lin CW, Sim S, Ainsworth A, Okada M, Kelsch W, Lois C (2010) Genetically increased cell-intrinsic excitability enhances neuronal integration into adult brain circuits. Neuron 65:32–39.

Liu S, Shipley MT (2008) Multiple conductances cooperatively regulate spontaneous bursting in mouse olfactory bulb external tufted cells. J Neurosci 28:1625–1639.

Livneh Y, Feinstein N, Klein M, Mizrahi A (2009) Sensory input enhances synaptogenesis of adult-born neurons. J Neurosci 29:86–97.

Lledo PM, Merkle FT, Alvarez-Buylla A (2008) Origin and function of olfactory bulb interneuron diversity. Trends Neurosci 31:392–400.

Macrides F, Schneider SP (1982) Laminar organization of mitral and tufted cells in the main olfactory bulb of the adult hamster. J Comp Neurol 208:419–430.

Madisen L, Mao T, Koch H, Zhuo JM, Berenyi A, Fujisawa S, Hsu YW, Garcia AJ 3rd, Gu X, Zanella S, Kidney J, Gu H, Mao Y, Hooks BM, Boyden ES, Buzsáki G, Ramirez JM, Jones AR, Svoboda K, Han X, Turner EE, Zeng H (2012) A toolbox of Cre-dependent optogenetic transgenic mice for light-induced activation and silencing. Nat Neurosci 15:793–802.

Manabe H, Mori K (2013) Sniff rhythm-paced fast and slow gamma-oscillations in the olfactory bulb: relation to tufted and mitral cells and behavioral states. J Neurophysiol 110:1593–1599.

Merkle FT, Fuentealba LC, Sanders TA, Magno L, Kessaris N, Alvarez-Buylla A (2014) Adult neural stem cells in distinct microdomains generate previously unknown interneuron types. Nat Neurosci 17:207–214.

Mori K, Kishi K and Ojima H (1983) Distribution of dendrites of mitral, displaced mitral, tufted, and granule cells in the rabbit olfactory bulb. J Comp Neurol 219: 339–355.

Mori K, Sakano H (2011) How is the olfactory map formed and interpreted in the mammalian brain? Annu Rev Neurosci 34:467–499.

Neher E (1992) Correction for liquid junction potentials in patch clamp experiments. Methods Enzymol 207:123–131.

Nithianantharajah J, Hannan AJ (2006) Enriched environments, experience-dependent plasticity and disorders of the nervous system. Nat Rev Neurosci 7:697–709.

Nusser Z, Kay LM, Laurent G, Homanics GE, Mody I. (2001) Disruption of GABA(A) receptors on GABAergic interneurons leads to increased oscillatory power in the olfactory bulb network. J Neurophysiol 86:2823–33.

Nunes D, Kuner T (2015) Disinhibition of olfactory bulb granule cells accelerates odour discrimination in mice. Nat Commun 6:8950.

Orona E, Scott JW, Rainer EC (1983) Different granule cell populations innervate superficial and deep regions of the external plexiform layer in rat olfactory bulb. J Comp Neurol 217:227–237.

Orona E, Rainer EC and Scott JW (1984) Dendritic and axonal organization of mitral and tufted cells in the rat olfactory bulb. J Comp Neurol 226: 346–356.

Ranjan A, Mallick BN (2010) A modified method for consistent and reliable Golgi-cox staining in significantly reduced time. Front Neurol 1:157.

Renier N, Wu Z, Simon DJ, Yang J, Ariel P, Tessier-Lavigne M. (2014) iDISCO: a simple, rapid method to immunolabel large tissue samples for volume imaging. Cell 159:896–910.

Rochefort C, Gheusi G, Vincent JD, Lledo PM (2002) Enriched odor exposure increases the number of newborn neurons in the adult olfactory bulb and improves odor memory. J Neurosci 22:2679–2689.

Saghatelyan A, Roux P, Migliore M, Rochefort C, Desmaisons D, Charneau P, Shepherd GM, Lledo PM (2005) Activity-dependent adjustments of the inhibitory network in the olfactory bulb following early postnatal deprivation. Neuron 46:103–116.

Sakamoto M, Imayoshi I, Ohtsuka T, Yamaguchi M, Mori K, Kageyama R (2011) Continuous neurogenesis in the adult forebrain is required for innate olfactory responses. Proc Natl Acad Sci USA 108:8479–8484.

Sakamoto M, Ieki N, Miyoshi G, Mochimaru D, Miyachi H, Imura T, Yamaguchi M, Fishell G, Mori K, Kageyama R, Imayoshi I (2014) Continuous postnatal neurogenesis

contributes to formation of the olfactory bulb neural circuits and flexible olfactory associative learning. J Neurosci 34:5788–5799.

Sanes JR, Lichtman JW (2001) Induction, assembly, maturation and maintenance of a postsynaptic apparatus. Nat Rev Neurosci 2:791–805.

Serizawa S, Miyamichi K, Takeuchi H, Yamagishi Y, Suzuki M, Sakano H (2006) A neuronal identity code for the odorant receptor-specific and activity-dependent axon sorting. Cell 127: 1057–1069.

Shepherd GM, Chen WR, Greer CA (2004) Olfactory bulb. In: The synaptic organization of the brain (Shepherd GM, ed), pp 165–216. Oxford: Oxford UP.

Southall PJ, Boxer GM, Bagshawe KD, Hole N, Bromley M, Stern PL (1990) Immunohistological distribution of 5T4 antigen in normal and malignant tissues. Br J Cancer 61:89–95.

Southgate TD, McGinn OJ, Castro FV, Rutkowski AJ, Al-Muftah M, Marinov G, Smethurst GJ, Shaw D, Ward CM, Miller CJ, Stern PL (2010) CXCR4 mediated chemotaxis is regulated by 5T4 oncofetal glycoprotein in mouse embryonic cells. PLoS One 5:e9982.

Torashima T, Yamada N, Itoh M, Yamamoto A, Hirai H (2006) Exposure of lentiviral vectors to subneutral pH shifts the tropism from Purkinje cell to Bergmann glia. Eur J Neurosci 24:371–380.

Tsuboi A, Yoshihara S, Yamazaki N, Kasai H, Asai-Tsuboi H, Komatsu M, Serizawa S, Ishii T, Matsuda Y, Nagawa F, Sakano H (1999) Olfactory neurons expressing closely linked and homologous odorant receptor genes tend to project their axons to neighboring glomeruli on the olfactory bulb. J Neurosci 19: 8409–8418.

Vernet-Maury E, Polak EH, Demael A (1984) Structure-activity relationship of stress-inducing odorants in the rat. J Chem Ecol 10: 1007–1018.

Whitman MC, Greer CA (2009) Adult neurogenesis and the olfactory system. Prog Neurobiol 89:162–175.

Yamaguchi M, Mori K (2005) Critical period for sensory experience-dependent survival of newly generated granule cells in the adult mouse olfactory bulb. Proc Natl Acad Sci U S A 102:9697–9702.

Yokoi M, Mori K, Nakanishi S (1995) Refinement of odor molecule tuning by dendrodendritic synaptic inhibition in the olfactory bulb. Proc Natl Acad Sci U S A 92:3371–3375.

Yoshihara S, Omichi K, Yanazawa M, Kitamura K, Yoshihara Y (2005) Arx homeobox gene is essential for development of mouse olfactory system. Development 132: 751–762.

Yoshihara S, Takahashi H, Nishimura N, Naritsuka H, Shirao T, Hirai H, Yoshihara Y, Mori K, Stern PL and Tsuboi A (2012) 5T4 glycoprotein regulates the sensory input-dependent development of a specific subtype of newborn interneurons in the mouse olfactory bulb. J Neurosci 32:2217–2226.

Yoshihara S, Takahashi H, Nishimura N, Kinoshita M, Asahina R, Kitsuki M, Tatsumi K, Furukawa-Hibi Y, Hirai H, Nagai T, Yamada K, Tsuboi A (2014) Npas4 regulates Mdm2 and thus Dcx in experience-dependent dendritic spine development of newborn olfactory bulb interneurons. Cell Rep 8:843–857.

Figure legends

Figure 1. 5T4 affects dendritic development in 5T4 GCs, but not in non-5T4 GCs. ***A, B***, Dendritic branching in 5T4 GCs (***A***) and non-5T4 GCs (***B***). A lentiviral vector carrying *CMVp—gapEYFP* was injected into the LVs of wild-type and *5T4*$^{-/-}$ mice at P3, and OB sections were immunostained with the GFP antibody (green), and the 5T4 or LacZ antibody (red) at P21. Scale bars, 50 μm. Enlarged photos of the area enclosed by a white square in an upper panel are shown below. Scale bars, 20 μm. White arrowheads indicate the cell bodies of 5T4 GCs and non-5T4 GCs. (***right***), The branching number of GC dendrites is expressed as the mean ± s.e.m. (ns {not significant, p = 0.6511}, and **p = 0.0002 between wild-type and *5T4*$^{-/-}$ mice [Student's *t* test]; n = 20 cells from three animals of each line). ***C***, IHC and ISH of wild-type OB sections with the BrdU antibody (green) and 5T4 probe (red), respectively. Scale bar, 40 μm. (***right***), The numbers of 5T4^{+} GCs and BrdU^{+} 5T4^{+} GCs are shown as the mean ± s.e.m. (n = 6 sections per bar in the graph from three animals). Note that 5T4 GCs are generated mainly during the embryonic (E15.5) and neonatal (P0) stages.

Figure 2. The morphology of OB projection neurons is not affected in *5T4* KO mice. ***A***, IHC of OB sections from the wild-type and *5T4*$^{-/-}$ mice at P56 with antibodies against 5T4 and LacZ, respectively. (***right***), The number of 5T4 GCs (5T4 or LacZ-positive) is expressed as the mean ± s.e.m. (ns {not significant, p = 0.201} between wild-type and *5T4*$^{-/-}$ mice [Student's *t* test]; n = 6 sections per bar from three animals). Scale bar, 20 μm. ***B***, IHC of OB sections from the wild-type and *5T4*$^{-/-}$ mice at P56 with antibodies against cholecystokinin (CCK) and PGP9.5. TC, tufted cell; MC, mitral cell. Scale

bar, 40 µm. (***right***), The areas of CCK^+ and $PGP9.5^+$ are expressed as the mean ± s.e.m. (ns {not significant, p = 0.864 (CCK^+) and 0.392 ($PGP9.5^+$)} between wild-type and *5T4*$^{-/-}$ mice [Student's *t* test]; n = 6 sections per bar from three animals). Note that the densities of MCs (PGP9.5-positive) and TCs (CCK-positive) are not remarkably different between wild-type and *5T4*$^{-/-}$ mice. ***C***, Golgi-Cox staining of OB sections from the wild-type and *5T4*$^{-/-}$ mice at P56–84. GL, glomerular layer; EPL, external plexiform layer; MCL, mitral cell layer. Scale bar, 40 µm.

Figure 3. Electrophysiological recordings classify external tufted cells (ETCs) into two types. ***A***, Sample current traces in the cell-attached configuration showing firing bursts recorded from three different bursting and non-bursting ETCs. ***B, D***, Two-dimensional projection of morphologies in a biocytin-labeled bursting (***B***) or non-bursting (***D***) ETC. Basal dendrites extending laterally in the superficial EPL are indicated by arrowheads. Scale bars, 20 µm. GL, glomerular layer; EPL, external plexiform layer. ***C, E***, Voltage traces in current-clamp mode from the bursting (***C***) and non-bursting (***E***) ETCs shown in (***B***) and (***D***), respectively. Spike trains elicited by depolarizing current injections showed noticeable accommodation. Voltage responses induced by hyperpolarizing current injections exhibited prominent sags (arrow) upon membrane hyperpolarization and rebound depolarization accompanied by burst firings (asterisk). ***F***, Sag ratios in two types of ETCs from wild-type and *5T4* KO mice. The bursting ETCs showed a significantly higher sag ratio to 30 mV hyperpolarization than the non-bursting ETCs in both wild-type and *5T4*$^{-/-}$ OBs (**p < 0.0001 compared between bursting and non-bursting ETCs; WT: bursting ETC, n = 17, non-bursting ETC, n = 20; *5T4* KO: bursting ETC, n = 17, non-bursting ETC, n = 19)

Figure 4. Optogenetic stimulation of *ChR2*-expressing 5T4 GCs in OB slices. ***A***, Expression of *ChR2-EYFP* in Ai32 mice injected with the *5T4p—Cre* lentiviral vector. IHC of OB sections with antibodies against GFP (green) and 5T4 (magenta). Scale bar, 40 μm. ***B***, Ratios of $EYFP^+$ $5T4^+$ GCs in $EYFP^+$ cells (***left***) and $EYFP^+$ $5T4^+$ GCs in $5T4^+$ GCs (***right***) are shown as the mean ± s.e.m. (n = 6 sections from two animals). ***C***, A schematic diagram of light-evoked $GABA_A$-PSCs recorded from an ETC. A superficial, upper half of the EPL near the recorded ETC was irradiated by light (10–15 ms in duration) to activate the ramified dendritic tufts of *ChR2*-expressing GCs. ***D***, Representative traces of light-evoked $GABA_A$-PSCs recorded from a non-bursting ETC. Thirteen traces including failures are superimposed. A horizontal bar represents light (455 nm) irradiation to the EPL. Note that the $GABA_A$-PSCs in bursting ETCs (***upper***) were completely abolished by SR95531 (an inhibitor of the $GABA_A$ receptor) (***lower***). ***E***, Ratios of cells showing light-evoked $GABA_A$-PSCs in bursting ETCs, non-bursting ETCs, and MCs. ***F***, Distribution of $GABA_A$-PSC amplitudes in bursting ETCs, non-bursting ETCs, and MCs. Note that the mean amplitudes of $GABA_A$-PSCs were indistinguishable between the three types.

Figure 5. GABAergic inputs are reduced in non-bursting ETCs from *5T4* KO mice. ***A***, Superimposed traces of spontaneous $GABA_A$-PSCs, with an amplitude larger than 40 pA, recorded from a non-bursting ETC in wild-type mice. Each trace is lined up at onset. ***B***, A schematic diagram of electrically evoked $GABA_A$-PSCs recorded from an ETC (***left***) or an MC (***right***). GCs were stimulated with a constant current (200 μs in duration) using a bipolar platinum electrode (50 μm in diameter) placed in the EPL.

Evoked $GABA_A$-PSCs were recorded from an ETC or an MC at a holding potential of -80 mV. ***C***, Representative traces of evoked $GABA_A$-PSCs recorded at different stimulus intensities (10–20 μA) from the non-bursting ETC. For each stimulus intensity, 20 traces are superimposed. ***D, E, F***, Plots for the amplitude of electrically evoked $GABA_A$-PSCs versus the stimulus intensity (increment from a threshold current) in bursting ETCs (***D***), non-bursting ETCs (***E***), and MCs (***F***) between wild-type (dotted lines) and *5T4* KO mice (solid lines). The amplitude of $GABA_A$-PSCs is expressed as ratios to the mean amplitude of stable-minimal PSCs. ***G, H, I***, Scatter plots for the mean amplitude (***upper***), integrated charge (***middle***) and coefficient of variation (***lower***) of evoked $GABA_A$-PSCs, recorded from bursting ETCs (***G***), non-bursting ETCs (***H***), and MCs (***I***) in wild-type and *5T4* KO mice (**p < 0.01, *p < 0.05 between wild-type and *5T4* KO mice [Mann-Whitney rank-sum test]; bursting ETCs: n = 18 cells from each line; non-bursting ETCs: n = 22 cells from each line; MCs: n = 23 cells from each line). Outlying data are shown as individual points with each numerical value. The internal bar and height of the box represent the median and interquartile range, respectively.

Figure 6. Excitatory inputs are reduced in 5T4 GCs from *5T4* KO mice. ***A***, A schematic diagram of electrically evoked EPSCs recorded from a 5T4 GC. ETCs were stimulated with a constant current (200 μs in duration) using a bipolar platinum electrode (50 μm in diameter) placed in the EPL. Evoked EPSCs were recorded from a 5T4 GC at a holding potential of -80 mV. ***B***, In wild-type OB slices, recorded cells were injected with biocytin (magenta) with a pipette and subjected to whole-mount IHC with the 5T4 antibody (green) to identify 5T4 GCs. Scale bar, 20 μm. ***C***, In *5T4*$^{-/-}$

OB slices, in which cells had been loaded with the LacZ substrate using a recording pipette, LacZ-positive GCs, namely, 5T4-derived GCs, were recorded. Differential interference contrast (***right***) and fluorescent (***left***) images of a LacZ-positive GC in the MCL are indicated under the conventional whole-cell configuration. Note that fluorescence became apparent after rupturing the cell membrane. Scale bar, 20 μm. ***D***, Representative traces of electrically evoked EPSCs recorded at different stimulus intensities (6–16 μA) from 5T4 GCs. For each stimulus intensity, 20 traces are superimposed. ***E***, Scatter plots for the mean amplitude (***left***) and coefficient of variation (***right***) of electrically evoked EPSCs recorded from 5T4-derived GCs in wild-type and *5T4* KO mice (**p = 0.0077 between wild-type and *5T4* KO mice [Mann-Whitney rank-sum test]; n = 16 (WT) and 17 (*5T4* KO) cells).

Figure 7. Detection thresholds for odors are higher in *5T4* KO mice. ***A***, A food finding test for wild-type and *5T4* KO mice. (***middle***), In the 1st and 2nd trials, times spent by the fasted mice in finding a food pellet buried at the same position under the bedding on one side of the test cage were measured at 1 hr intervals between the two trials. One hour later, the 3rd trial was performed without a food pellet, and the investigation time in each area during the 2 min test was measured. (***right***), Bars depict the difference in time taken by the mice to investigate each area of the cage in the 3rd trial. Note that wild-type and *5T4* KO mice could not be distinguished based on food-seeking times, expressed as the mean ± s.e.m. (ns {not significant, p = 0.709 (1st), 0.082 (2nd) and 0.186 (3rd)} between wild-type and *5T4* KO mice [Welch *t* test with Holm-Bonferroni correction]; n = 7 (WT) and 8 (5T4 KO) animals). ***B***, An olfactory habituation-dishabituation test for the wild-type and *5T4*

KO mice. First, clean air was supplied into the test cage, and mice were habituated for 15 min. In the 1st trial, clean air was supplied for 3 min. Differences in investigation times between the 1st trial and 2nd trial with eugenol are expressed as the mean ± s.e.m. (ns {not significant, p = 0.275 (0.63 μM) and 0.463 (630 μM)}, and * {significant, p = 0.000001 (6.3 μM) and 0.007 (63 μM)} between wild-type and *5T4* KO mice [Welch *t* test with Holm-Bonferroni correction]; n = 5 animals in each condition). ***C***, An olfactory avoidance test for wild-type and *5T4* KO mice. Mice were transferred to the test cage and exposed to a filter paper scented with three different amounts (0, 4 and 40 μl) of nTMT. Freezing time and avoidance index during the 10 min test are expressed as the mean ± s.e.m. (*p = 0.008 (freezing) and 0.014 (avoidance) between wild-type and *5T4* KO mice [Welch *t* test with Holm-Bonferroni correction]; n = 5 animals in each condition). ***D***, An object recognition test for wild-type and *5T4* KO mice. Object exploration times for animals presented with either two identical (habituation phase: object A) or two different (test phase: object A and B) objects are expressed as the mean ± s.e.m. (*p = 0.006 (WT) and 0.008 (5T4 KO) between *right* and *left* objects [a Wilcoxon signed-rank test]; n = 11 (WT) and 9 (5T4 KO) animals).

Figure 8. Discrimination learning between two different odors is impaired in *5T4* KO mice. ***A***, An odor-discrimination learning test. The top schema indicates the experimental time course. In the training phase on Day 1–6, wild-type and *5T4* KO mice learned to associate the sugar reward with odor A. In the test phase on Day 5–7, the sugar reward was removed from odor A, followed by odor-discrimination learning (Test 1–3). The time taken by the mice to dig at each side of the test cage was measured. ***B***, Digging times during the 5-min test (Test 1–3) are represented as bar

graphs: eugenol paired with the sugar reward (red) and pentanol unpaired (blue). In Test 2 and 3, digging times in the area without odors (white bars) are expressed as the mean ± s.e.m. (**p = 0.000001 (Test 1, WT), 0.00001 (Test 2, WT) and 0.000006 (Test 2, 5T4 KO) between both areas in each test [a two-way repeated-measures ANOVA]; n = 5 animals from each line). ***C***, Digging times during the 5-min test (Test 1–3) are represented as bar graphs: (+) carvone paired with the sugar reward (red) and (-) carvone unpaired (blue). Digging times are expressed as the mean ± s.e.m. (**p = 0.001 (Test 1, WT) and 0.008 (Test 2, WT), and *p = 0.0169 (Test 2, 5T4 KO) between both areas in each test [a two-way repeated-measures ANOVA]; n = 5 animals from each line).

Figure 9. *5T4* KO mice cannot discriminate food odor in the presence of a background odor. ***A***, Double ISH with RNA probes to *5T4* (green) and *cFos* (neuronal activity marker, magenta) genes in OB sections from P21 odor-stimulated mice. *cFos* expression was induced immediately in 5T4 GCs after stimulation with the odorant amyl acetate for 30 min. Scale bar, 40 μm. ***B***, Ratios of $cFos^{+}$ $5T4^{+}$ GCs in $5T4^{+}$ GCs are shown as the mean ± s.e.m. (**p = 0.00009 compared with the pre-treatment condition [Student's *t* test]; n = 6 sections per bar from three animals). ***C***, A food finding test was performed in the presence of the food-unrelated odorant amyl acetate. (***middle***), In the 1st and 2nd trials, the times taken by the fasted mice to find a food pellet buried at the same position under the bedding in one side of the test cage were measured at a 1-hr interval between them. One hour later, the 3rd trial was performed without a food pellet, and the time spent by the mice in each side of the cage was measured during the 2-min test. (***right***), Bars depict the difference in time taken by the

mice to investigate each area of the cage in the 3rd trial. Compared with wild-type mice, *5T4* KO mice needed longer food-seeking times, which are expressed as the mean ± s.e.m. (ns {not significant, p = 0.371 (2nd) and 0.426 (3rd)}, and *p = 0.010 between wild-type and *5T4* KO mice [Welch *t* test with Holm-Bonferroni correction]; n = 13 (WT) and 8 (5T4 KO) animals).

Figure 10. Olfactory behaviors are also impaired in OB-specific *5T4* knockdown (KD) mice. ***A***, 5T4 protein production in wild-type and OB-specific *5T4* KD mice. Lentiviral vectors carrying three kinds of *H1p—5T4-shRNAs* were injected into both LVs and OBs of wild-type mice at P1. OB sections were immunostained with the 5T4 antibody (green) at P21. Scale bar, 40 μm. (***right***), Signal intensity of 5T4 within the EPL is expressed as the mean ± s.e.m. (**p = 0.009 compared with the control OBs [a Student's *t* test]; n = 6 sections from three animals in each line). ***B***, Two successive olfactory habituation-dishabituation tests for *5T4* KD mice. Differences in investigation times between the 1st trial and 2nd trial using eugenol at two different concentrations (Test 1, 6.3 μM; Test 2, 630 μM) are expressed as the mean ± s.e.m. (ns {not significant, p = 0.508}, and *p = 0.0007 between control and *5T4* KD mice [Welch *t* test with Holm-Bonferroni correction]; n = 12 (control) and 11 (5T4 KD) animals). ***C***, An olfactory avoidance test for *5T4* KD mice. Mice were transferred to the test cage and exposed to a filter paper scented with nTMT in three different amounts (0, 4, and 40 μl). Freezing time and avoidance index during the 10 min test period are expressed as the mean ± s.e.m. (*p = 0.002 between control and *5T4* KD mice [Welch *t* test with Holm-Bonferroni correction]; n = 5 animals in each condition). ***D***, An odor-discrimination learning test for *5T4* KD mice. Digging times during the 5 min

test (Test 1–3) are represented as bar graphs: eugenol paired with the sugar reward (red) and pentanol unpaired (blue). Digging times are expressed as the mean ± s.e.m. (**p = 0. 00005 (Test 1, control), 0.00005 (Test 2, control) and 0.00002 (Test 2, 5T4 KD) between both areas in each test [a two-way repeated-measures ANOVA]; n = 5 animals from each line).

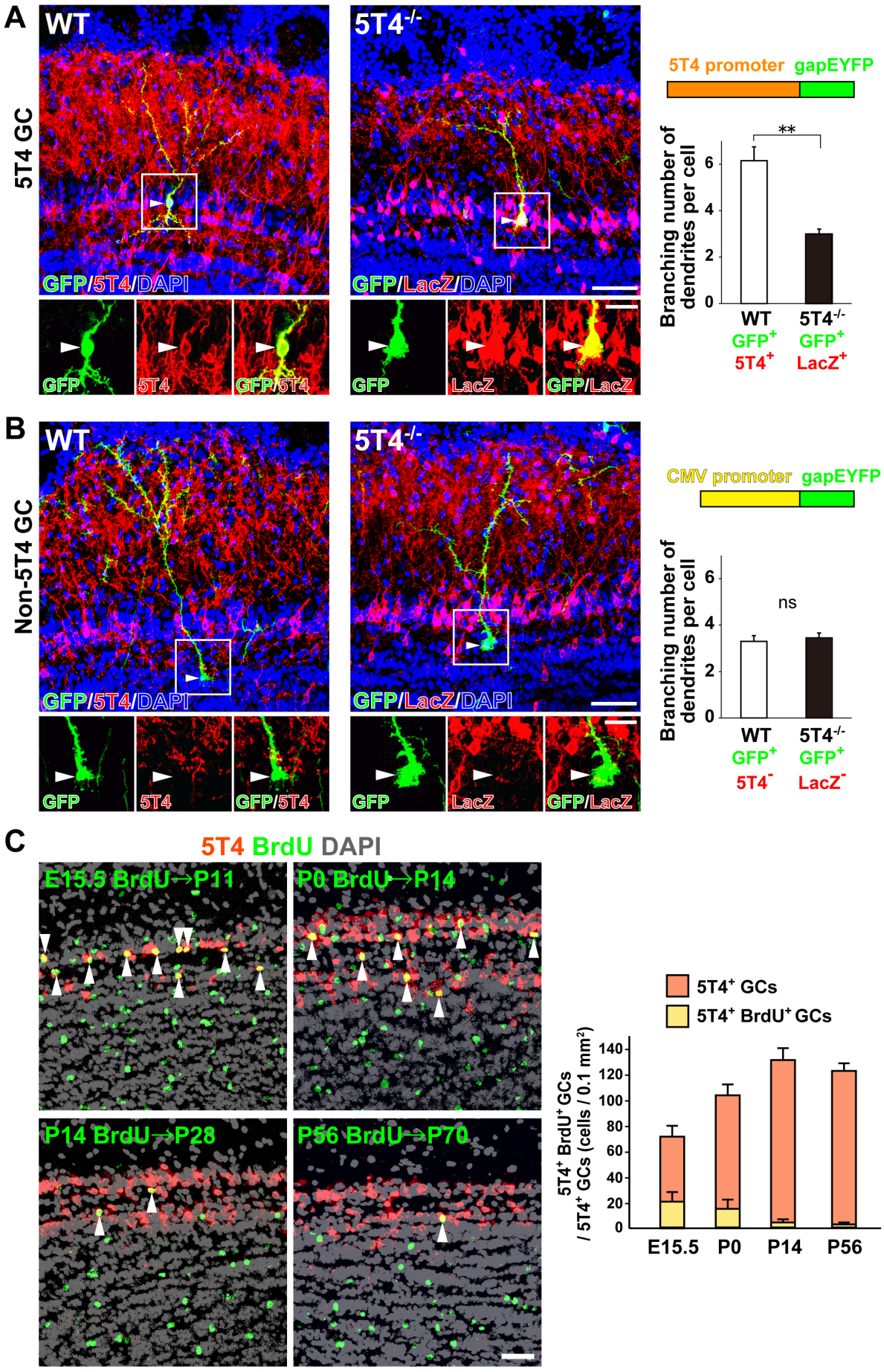

Figure 1 (Takahashi et al.)

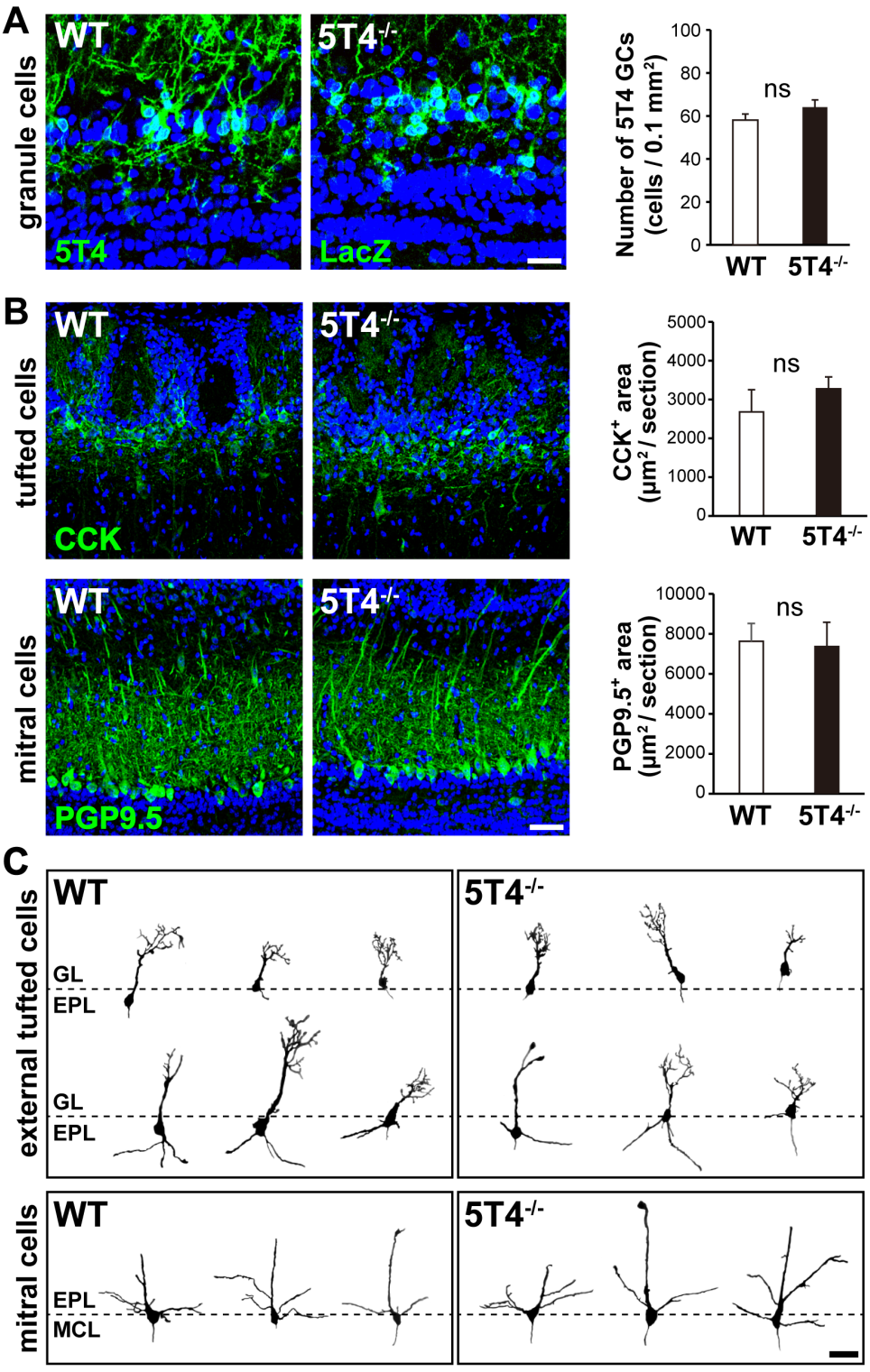

Figure 2 (Takahashi et al.)

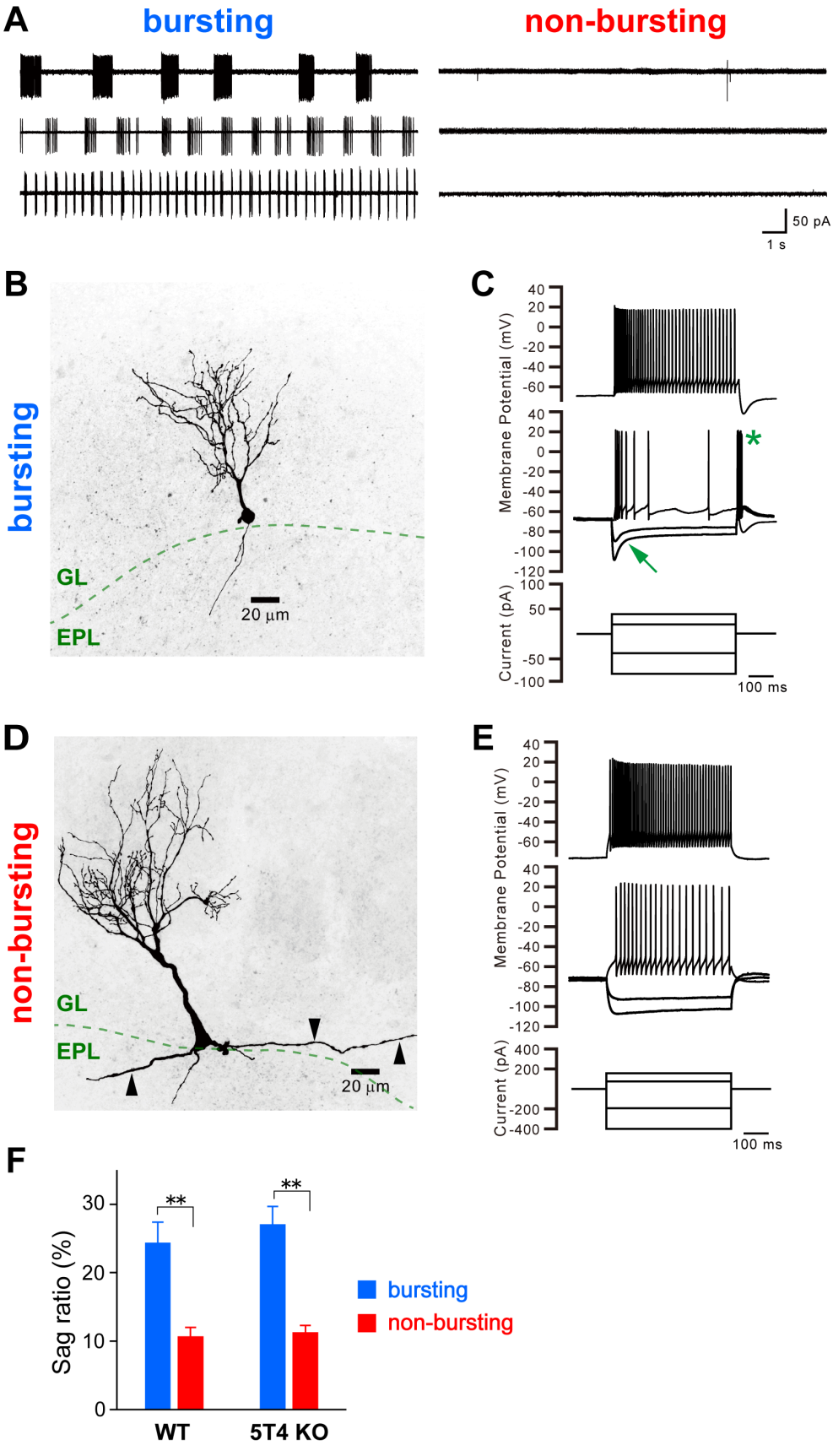

Figure 3 (Takahashi et al.)

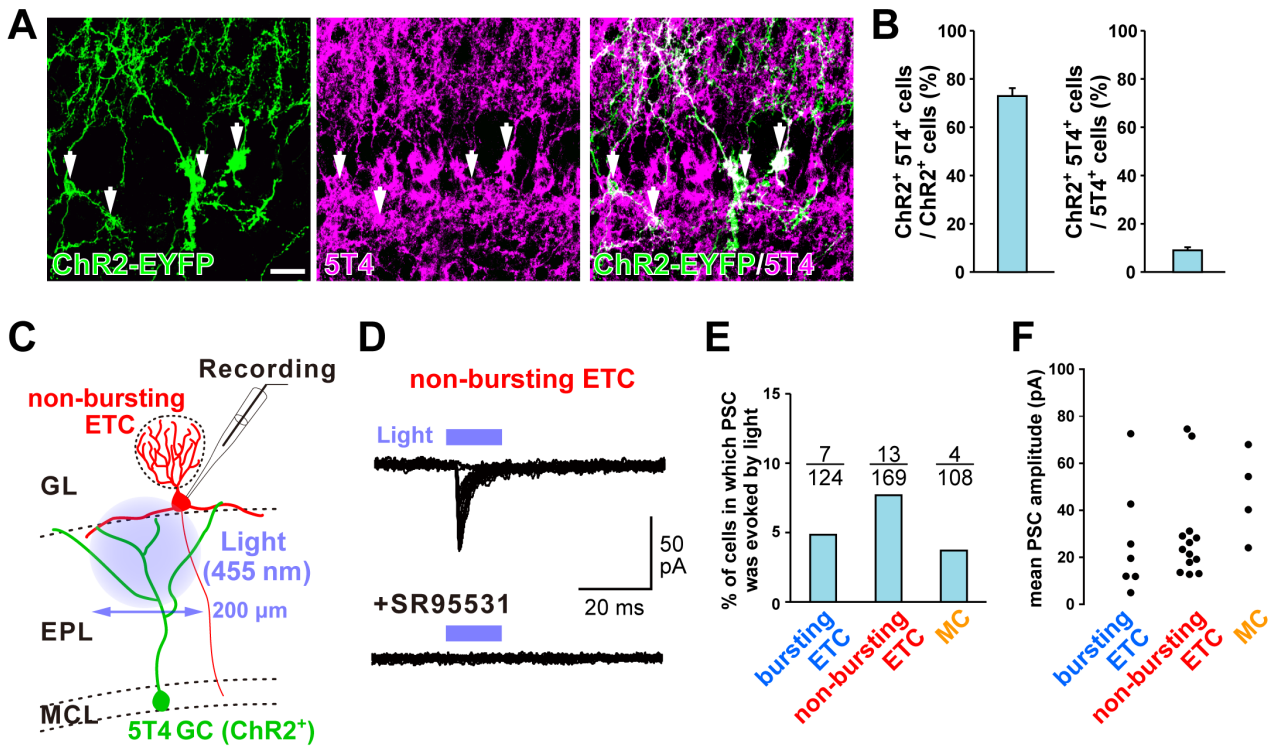

Figure 4 (Takahashi et al.)

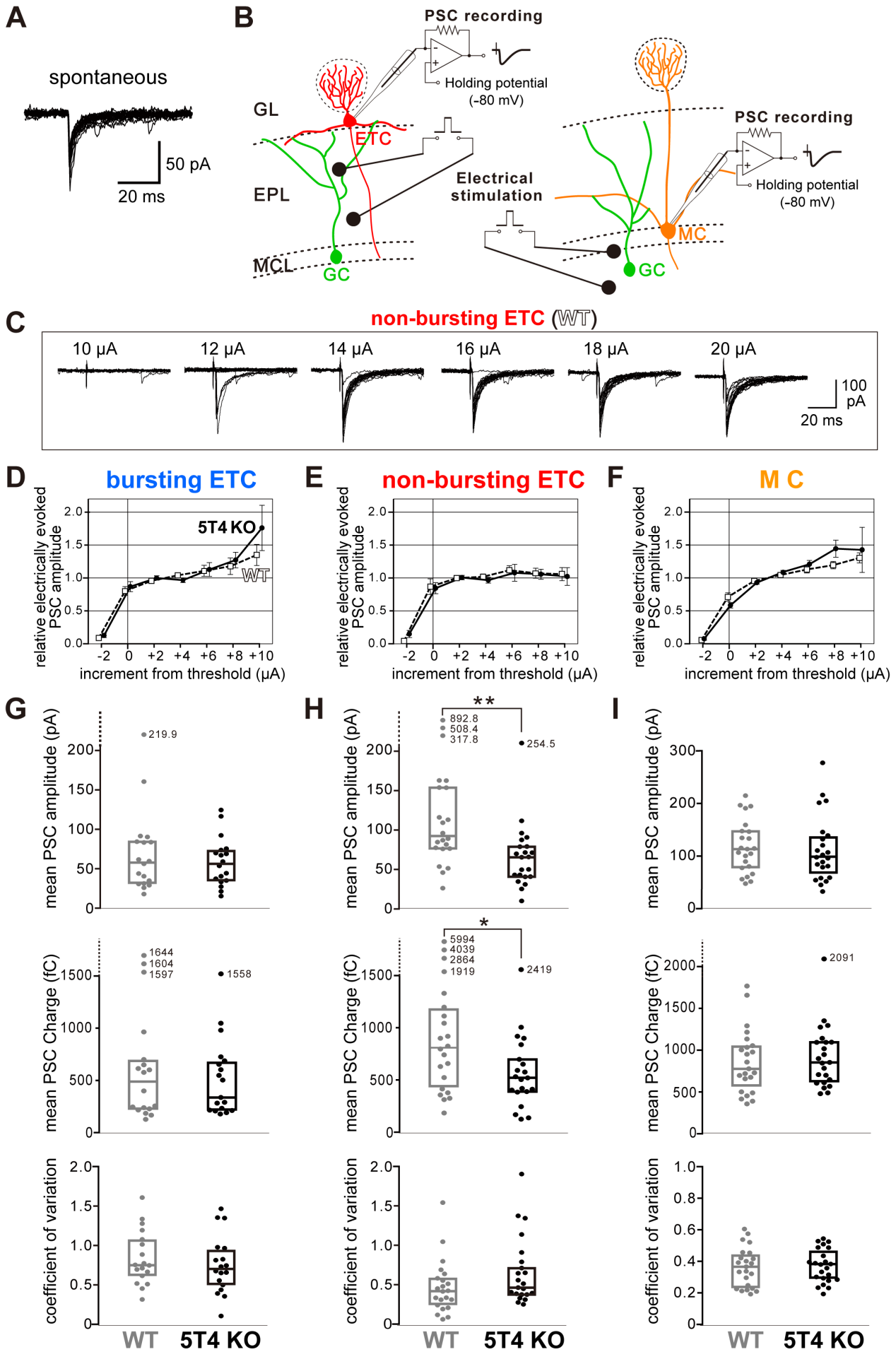

Figure 5 (Takahashi et al.)

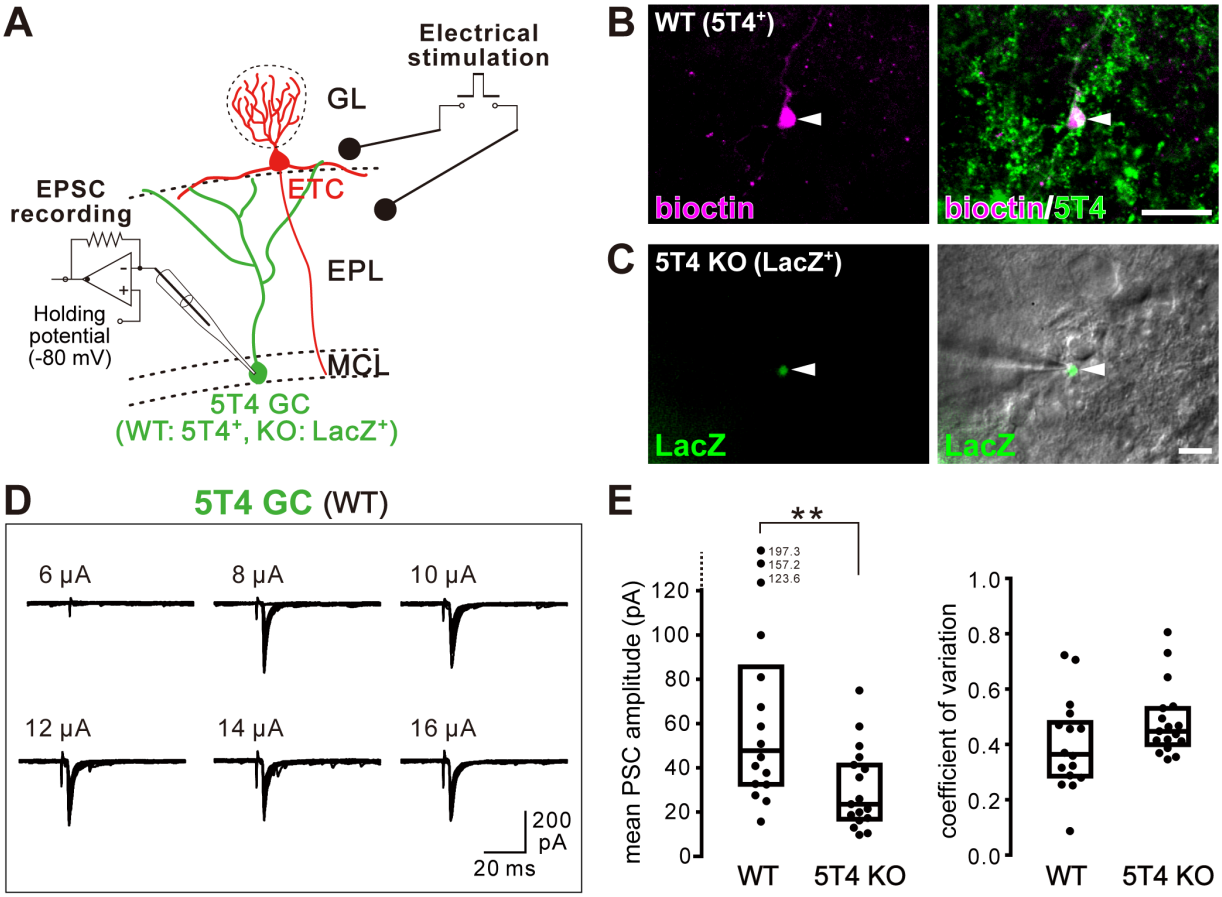

Figure 6 (Takahashi et al.)

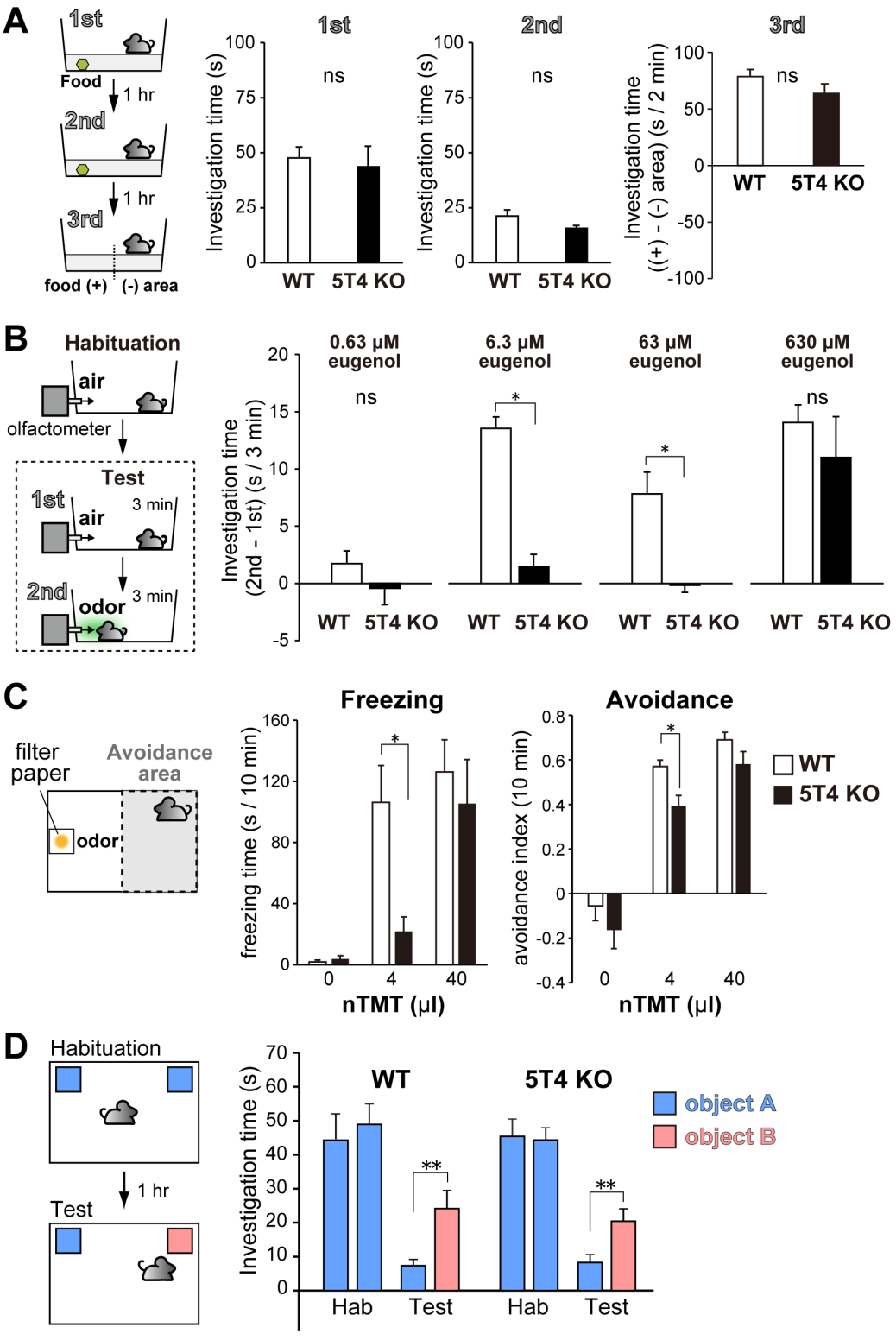

Figure 7 (Takahashi et al.)

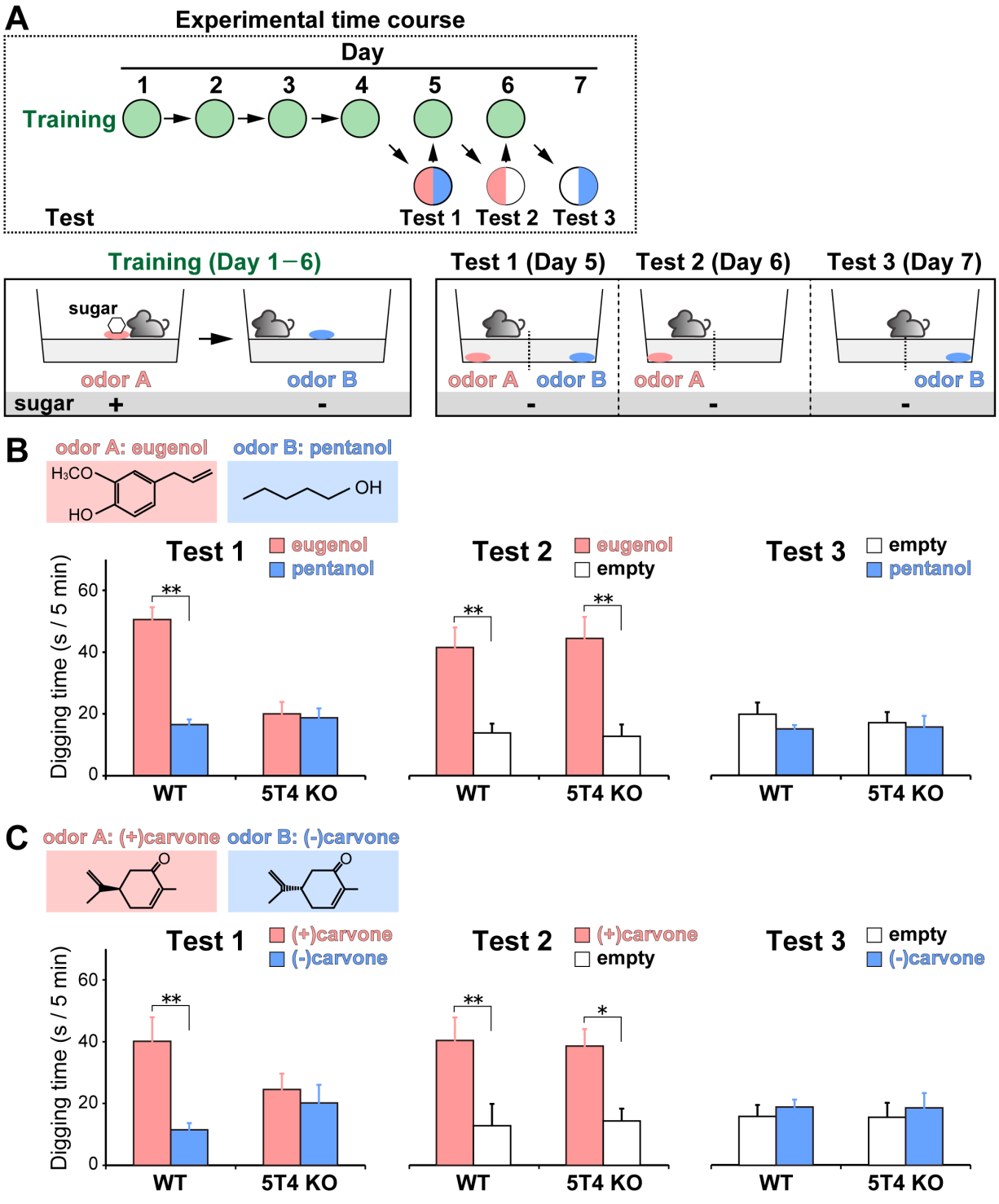

Figure 8 (Takahashi et al.)

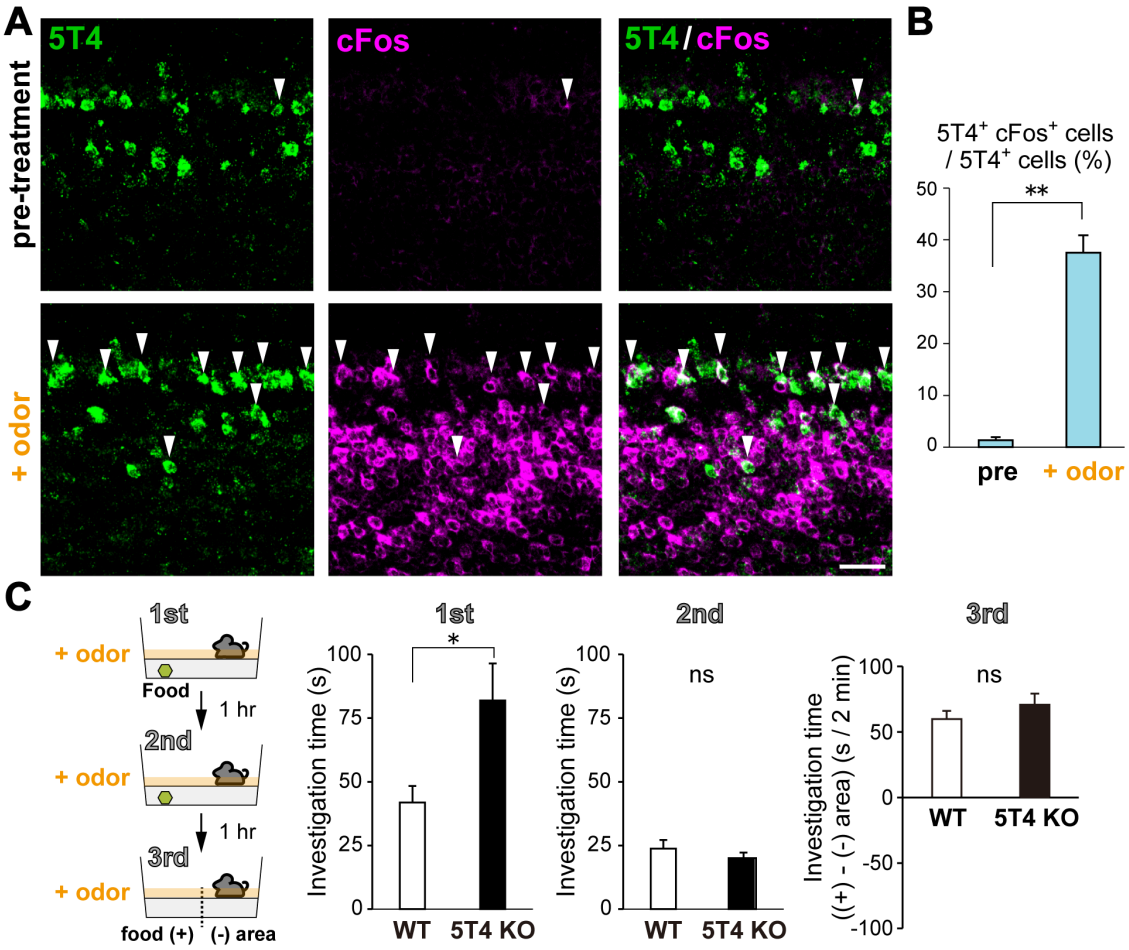

Figure 9 (Takahashi et al.)

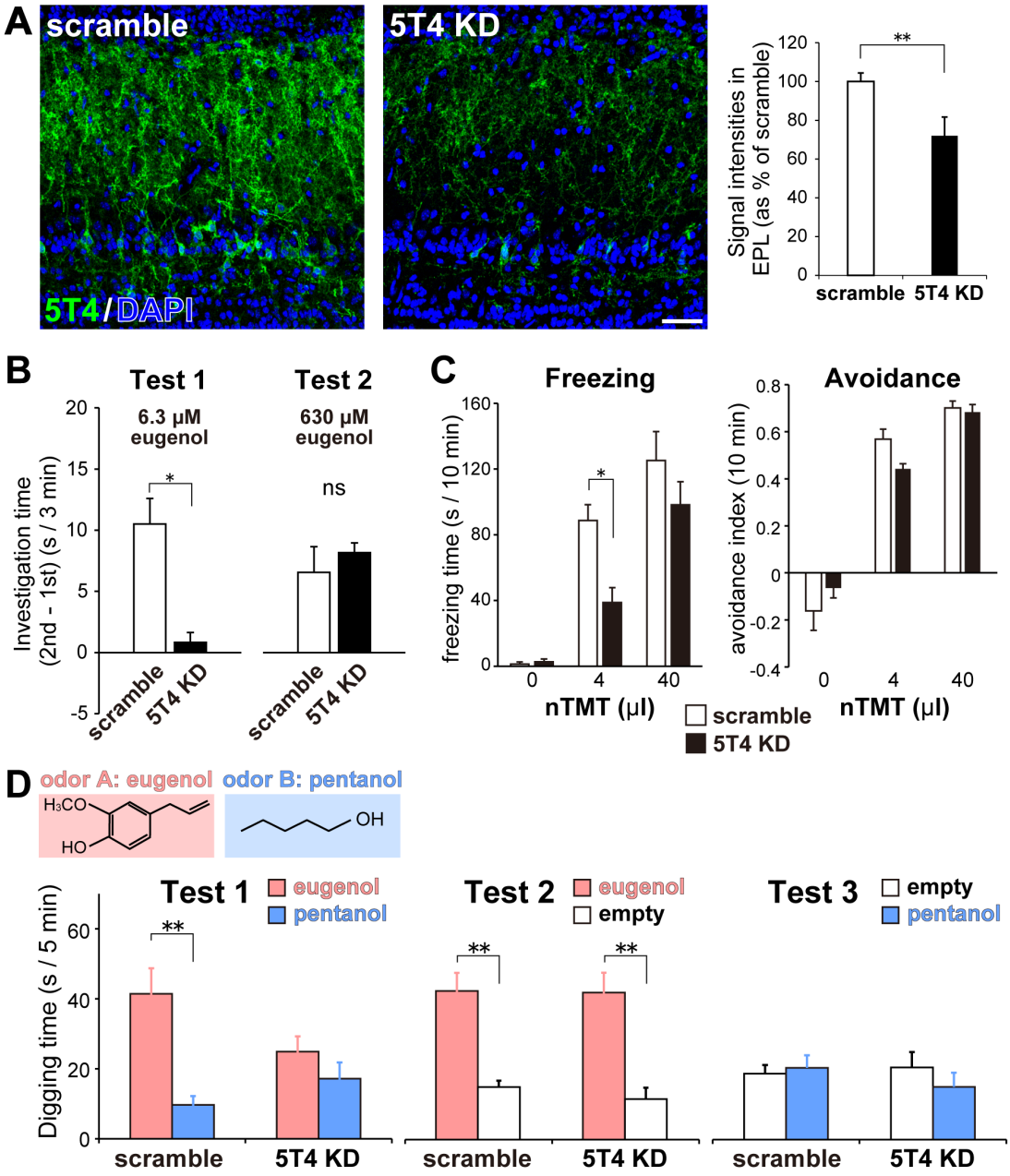

Figure 10 (Takahashi et al.)